

Generating LEVs on Energetically Optimal, Flapping Wing Designs by Modulating Leading Edge Angle

David J. Willis*

University of Massachusetts, Lowell, Lowell, MA 01854, U.S.A.

Per-Olof Persson†

University of California, Berkeley, Berkeley, CA 94720-3840, U.S.A.

In this paper a series of two- and three-dimensional, multi-fidelity computational models are presented and used in a preliminary exploration of leading edge vortex (LEV) evolution on pitching and plunging wings. The lower fidelity computational tools (thin airfoil theory and doublet lattice method) are framed in a quasi-inverse design context to determine the wing shape (twist and camber) that achieve a prescribed (leading and trailing edge) shed vorticity footprint. A high-order, computational fluid dynamics tool is used to simulate the final wing geometries.

A series of preliminary results of increasing complexity and relevance to flapping wings are presented to demonstrate the viability of the lower fidelity quasi-inverse wing design methods. First a two-dimensional pitch-ramp case is presented to illustrate the impact of leading edge angle as well as leading and trailing edge vorticity shedding rate on the generation and persistence of LEVs. The second exploration considers a two-dimensional model of flapping downstroke motion (simple half cycle of a sinusoidal heave). Finally, some preliminary results using similar quasi-inverse design methods in three-dimensions are presented. While preliminary, the results of our investigations illustrate that LEVs can be modulated using an appropriate combination of wing local camber and incidence angle.

I. Background

The discovery of near wing flow structures (e.g. LEVs) on insect wings has revolutionized the fundamental comprehension of low-Reynolds number flapping flight.¹⁻⁶ Since their discovery, these near-wing flow structures have been examined and observed for insects using: observational animal-flight experiments,^{1,3,7} physical laboratory experiments,^{2,5,8-10} and computations.^{11,12} These studies have revealed insect-like flyers use leading and trailing edge flow structures to augment lift and improve maneuverability.

The existence and role of LEV's in larger animals flying at moderate Reynolds numbers (e.g. bats and birds, $Re \simeq 5,000 - 50,000$) is less well understood. Until recently, it was not even clear whether these flyers employed LEVs for augmenting lift production.¹³ In the past decade however, LEV structures have been observed in the laboratory for small and medium sized bats¹⁴ and birds,^{15,16} indicating that these near-wing flow structures have some relevance in regimes other than insect flight. Most of these observations have been made at slower flight speeds on actual animals.

Because of the challenges associated with experimentally capturing LEVs during natural flight, much of the experimental and computational effort to understand their behavior has focused on LEV generation using prescribed geometries and prescribed kinematics.^{2,11,12,17,18} These investigations explore the generation of LEVs on flat plates, insect wing models or flexible wings. While many of these studies have led to a deeper appreciation of LEV evolution, the experiments rely largely on the reaction of the fluid to the prescribed motion and prescribed shape of the immersed object. As such, the LEVs that have been examined in the

*Assistant Professor, Department of Mechanical Engineering, University of Massachusetts, Lowell, Lowell, MA 01854. E-mail: david_willis@uml.edu. AIAA Member.

†Assistant Professor, Department of Mathematics, University of California, Berkeley, Berkeley CA 94720-3840. E-mail: persson@berkeley.edu. AIAA Member.

laboratory could potentially be uncharacteristic of the desired flow structures or may not be as controllable as desired for understanding LEV evolution and development.

In this paper, we prototype a different approach for understanding LEVs – one that examines the leading and trailing edge shedding rate as the primary design criteria using an quasi-inverse design framework. In this approach, we are able to modulate the LEV and TEV systems to achieve the desired impact on the flow field; thereby allowing us to control and explore the flow features. We introduce the wing shape using variables (local incidence/twist and camber) that can be modulated to produce the desired vorticity shedding rate. This approach effectively inverts the traditional problem from a prescribed wing shape to a prescribed footprint in the fluid, potentially resulting in more control over the flow structure being examined in the virtual/computational environment.

II. Theory

From a fluid dynamics standpoint, we hypothesize that the leading edge and trailing edge vorticity shedding rates are significant factors in the development, evolution and persistence of LEV and TEV flow structures. As such, devising approaches for modulating the LEV and TEV shedding rates is desirable because the vorticity shed into the domain by a flapping or rotating wing (e.g. propeller) system is effectively a footprint of the energetics and force production. By mitigating the production of excess vorticity, a more efficient wing shape/kinematics can be defined, while shedding vorticity at desired span-wise locations of the wing, may result in more or less stable near-wing flow structures. In this paper, we examine the quasi-inverse problem of how to determine wing shapes that shed the desired amount of vorticity from either/both the leading and/or trailing edge of a wing.

When prescribing wing shed vorticity in a potential flow setting, Kelvin’s circulation theorems must be satisfied since they dictate the balance of vorticity. In the case of a flapping wing, the net vorticity in the domain and bound on the wing must sum to zero – resulting in a key balance of vorticity between the bound and shed vortex systems (Figure 1):

$$\Gamma_{Shed} = -\Gamma_{Wing} = \Gamma_{LEV} + \Gamma_{TEV} \quad (1)$$

Similarly:

$$\frac{\partial \Gamma_{Shed}}{\partial t} = -\frac{\partial \Gamma_{Wing}}{\partial t} = \frac{\partial \Gamma_{LEV}}{\partial t} + \frac{\partial \Gamma_{TEV}}{\partial t} \quad (2)$$

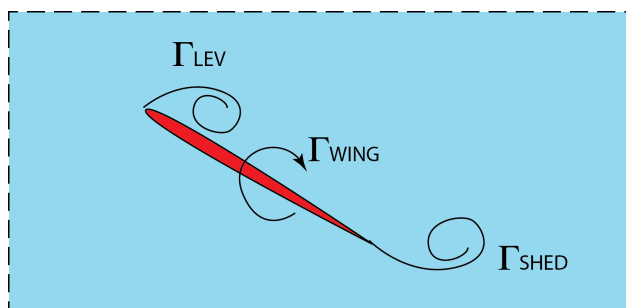


Figure 1. A two-dimensional slice of an arbitrary wing with both leading and trailing edge shedding. The dashed lines indicate the control volume under consideration.

From these simple vorticity shedding relationships, we can observe that the LEV strength is controlled by:

1. Vorticity shedding rate from the wing into the domain (i.e. trailing edge Kutta condition)
2. Vorticity generation rate at the leading edge (i.e. leading edge shedding criteria).
3. The balance or division of circulation between the wing, TEV system and LEV .

When prescribing the vorticity shed from a wing or airfoil, Kelvin’s circulation theorem must be satisfied. In addition to this, careful consideration of the location and strength of the shed vorticity must be made

to ensure efficient flight. The location and strength of the shed vorticity is directly related to the force generation and energy expenditure.

III. Computational Methods & Geometry Definition

We use a multi-fidelity computational framework for bio-inspired flapping flight to develop the wing shapes examined in this paper. The framework we have developed is the flapping wing analogy of the traditional fixed wing design framework – starting with a wake-only approach (similar to a Trefftz Plane analysis), transitioning to a potential flow analysis for preliminary geometry definition^{19,20} and ending with a fully defined wing geometry simulated using high order methods.²¹

III.A. Two-Dimensional Geometry Definition & Computational Methods

III.A.1. Two-Dimensional Geometry Definition

A simple cambered airfoil geometry is defined for the two-dimensional cases presented in this paper. The camber of the airfoil is defined using the angle θ . The airfoil mean camber-line is represented using a Hermite cubic spline with a leading edge angle θ , and a trailing edge angle $\theta/2$. The airfoil pitch angle, α is prescribed after the camber has been applied to the airfoil shape, and is defined as the angle between the horizontal and a line joining the leading and trailing edges. For the potential flow analysis, a thin-airfoil theory approach is employed, hence, an infinitely thin airfoil is used (see Figure 2, a-c). For the Navier-Stokes simulations presented in this paper, the airfoil has a prescribed thickness of 5% of the chord length ($t/c = 5\%$) with a semi-circular leading and trailing edge (see Figure 2, d-f).

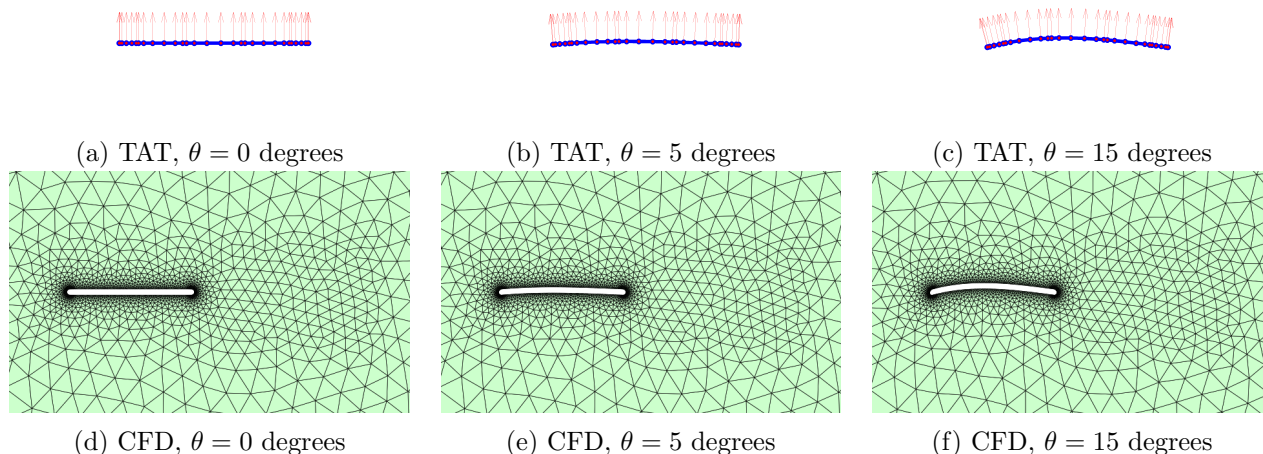


Figure 2. The airfoil geometry used in the 2-Dimensional simulations. (a) - (c) shows the thin airfoil theory geometry including the nodes and normal vectors (for illustrative purposes mesh is much coarser than actual discretization), while (d)-(f) illustrate the CFD geometry and mesh.

III.A.2. Two-Dimensional Wake-Only Method

In order to determine the optimal vorticity distribution in the domain left in the wake of a flapping wing, we use a two-dimensional version of the wake-only method²²⁻²⁴ To perform this wake-only analysis, a simple harmonic wake of the form:

$$h(t) = h_o \cos(\omega t) \quad (3)$$

must be defined, where h_o is half of the peak-to-peak flapping amplitude, and ω is the prescribed flapping frequency. In addition to the wake shape, the desired lift and thrust coefficients are prescribed as constraints to the optimization problem.²³ The wake-only method can then used to determine the optimal wake-

circulation distribution on the defined wake shape by solving the constrained quadratic functional:

$$\Gamma = \operatorname{argmin}(P_T), \text{ s.t. } C_T = a, \text{ and } C_L = b \quad (4)$$

In this paper, we consider an example where $C_L = 0$ with three different prescribed thrust coefficients, $C_T = 0.25, 0.50$ and 0.75 . For each of these thrust coefficients, the flapping amplitude was prescribed ($h_o = 1.25$) and a variety of different flapping Strouhal numbers were examined to determine the minimum power Strouhal number. The power coefficient as a function of the prescribed global flapping kinematics are shown in figure 3.

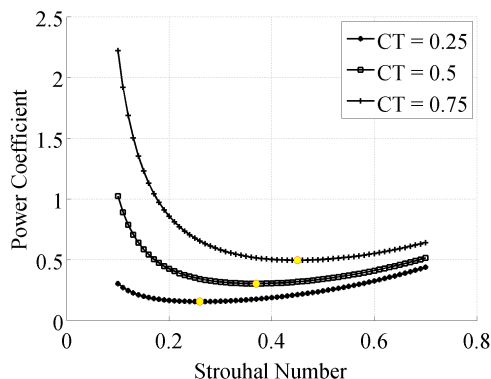


Figure 3. The power coefficient variation as a function of the Strouhal number for three different prescribed thrust coefficients, predicted using the one-dimensional wake-only method. The minimum power coefficient is presented.

The kinematics corresponding to the lowest predicted power coefficient were selected for further study. The circulation distribution in the wake of each of these three selected target wakes is shown in figure 4. The wake circulation distribution represents the net circulation in the fluid domain when the wing passes by that location. The net shed vorticity is the derivative of the net circulation with respect to time.

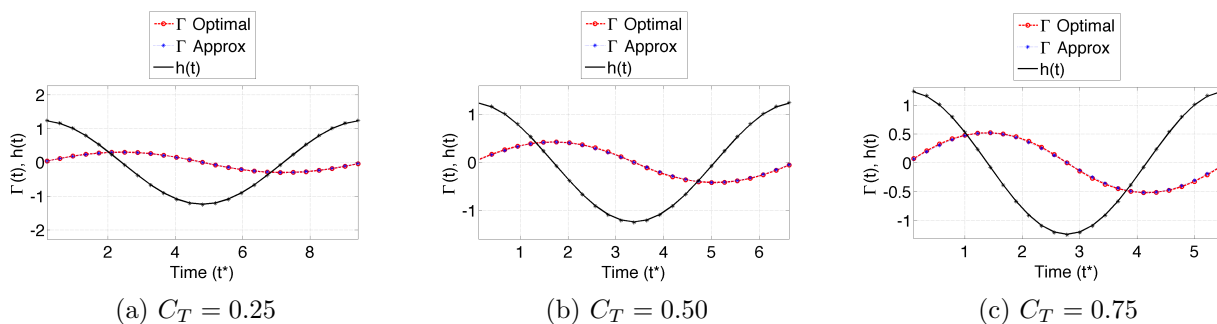


Figure 4. The wing kinematics and the optimal wake-circulation distribution for the three example thrust producing flapping wings.

Simple harmonic functions were applied to these optimal wake-only results to fit the wake data. Table 1 summarizes the optimal wake only results:

Table 1. Summary of the optimal wake-only results.

Thrust Coefficient	Strouhal Number	$\hat{\Gamma}$
0.25	0.26	0.3017
0.50	0.37	0.4220
0.75	0.45	0.5191

III.A.3. Two-Dimensional Thin Airfoil Theory Design Code

In principle, any efficient lower order potential flow method can be used for the two-dimensional airfoil shape determination. In this paper, we present a modification of a thin-airfoil-theory approach proposed by Gopalrathnam et al.^{19,25–27} We refer the reader to the detailed documentation, and only highlight how our quasi-inverse design approach uses and differs from their original implementation.

The thin-airfoil method presented by Gopalrathnam et al.^{25–27} has been implemented both in evaluation mode and design mode. In both the evaluation and the design mode, the total circulation and the leading edge suction parameter (LESP) matching form residual equations which must be satisfied at each timestep:

$$\begin{aligned} R_1 &= (\Gamma_{le} + \Gamma_{te} + \Gamma_{bound}) \rightarrow 0 \\ &\text{if, } LESP_{Calc} > LESP \\ R_2 &= LESP_{Calc} - LESP_{Crit} \rightarrow 0 \end{aligned}$$

The three modes of operation of the modified thin-airfoil theory code are briefly described below.

1. **Evaluation Mode:** The evaluation mode is the same method as that proposed by Gopalrathnam et al.^{25–27} which requires the user to input the wing geometry and kinematics at all time steps. The strength of the newly shed vorticity at the leading and trailing edges is determined by ensuring the residuals, R_1 and R_2 are approximately zero. While small differences likely exist between our implementation and the original, our thin-airfoil-theory evaluation mode is similar in principle. The only significant difference is the inclusion of a time varying camber capability in our approach as compared with the original implementation.
2. **Quasi-Inverse Design Mode:** We have extended the evaluation mode of the thin-airfoil theory to perform a quasi-inverse design suited to tailoring leading and trailing edge vortex strength. In this design mode, the leading and trailing edge shed vortex strengths are prescribed at each time step, and the wing shape (camber and incidence angle) that produces this shed vorticity is subsequently determined. In order to highlight the approach, we present an operational flow chart of the quasi-inverse design approach in figure 5. Many of the evaluation mode routines are re-used.
3. **Semi-Inverse Design Mode:** We have also extended the evaluation mode of the thin-airfoil theory to perform a semi-inverse design mode suited to solving for leading edge vortex strength when the airfoil camber is prescribed as a function of time. In this mode, the airfoil camber and trailing edge shed vorticity strength are prescribed, and the shed leading edge vorticity and the incidence angle are solved in the non-linear solution routine. Since this mode is not used in this paper, we do not describe it in detail; however, in principle, the thin airfoil theory can be cast in different ways to achieve the desired design problem solution.

In order to use the thin airfoil theory to model leading edge separation, a leading edge suction parameter for different camber wings must be determined. This is presented in the following section.

III.A.4. LESP as a Function of Camber

The leading edge suction parameter proposed by Gopalrathnam et al.^{25–27} was used in order to identify and appropriately model the shed vorticity at the leading edge of the airfoil. In this approach, an LESP parameter must be determined from a higher fidelity source, such as CFD or experiment. We employed CFD²¹ and XFOIL²⁸ calculations to determine the LESP for the different airfoil cambers. The results are presented in figure 6. The value of the LESP varies approximately linearly as a function of the airfoil camber angle for small camber angles. For larger camber angles, trailing edge separation results in less definitive values. This result is consistent across the two Reynolds numbers considered.

For our implementation, we fit the LESP values as a function of airfoil camber using a cubic polynomial between $-70^\circ < \theta < 70^\circ$.

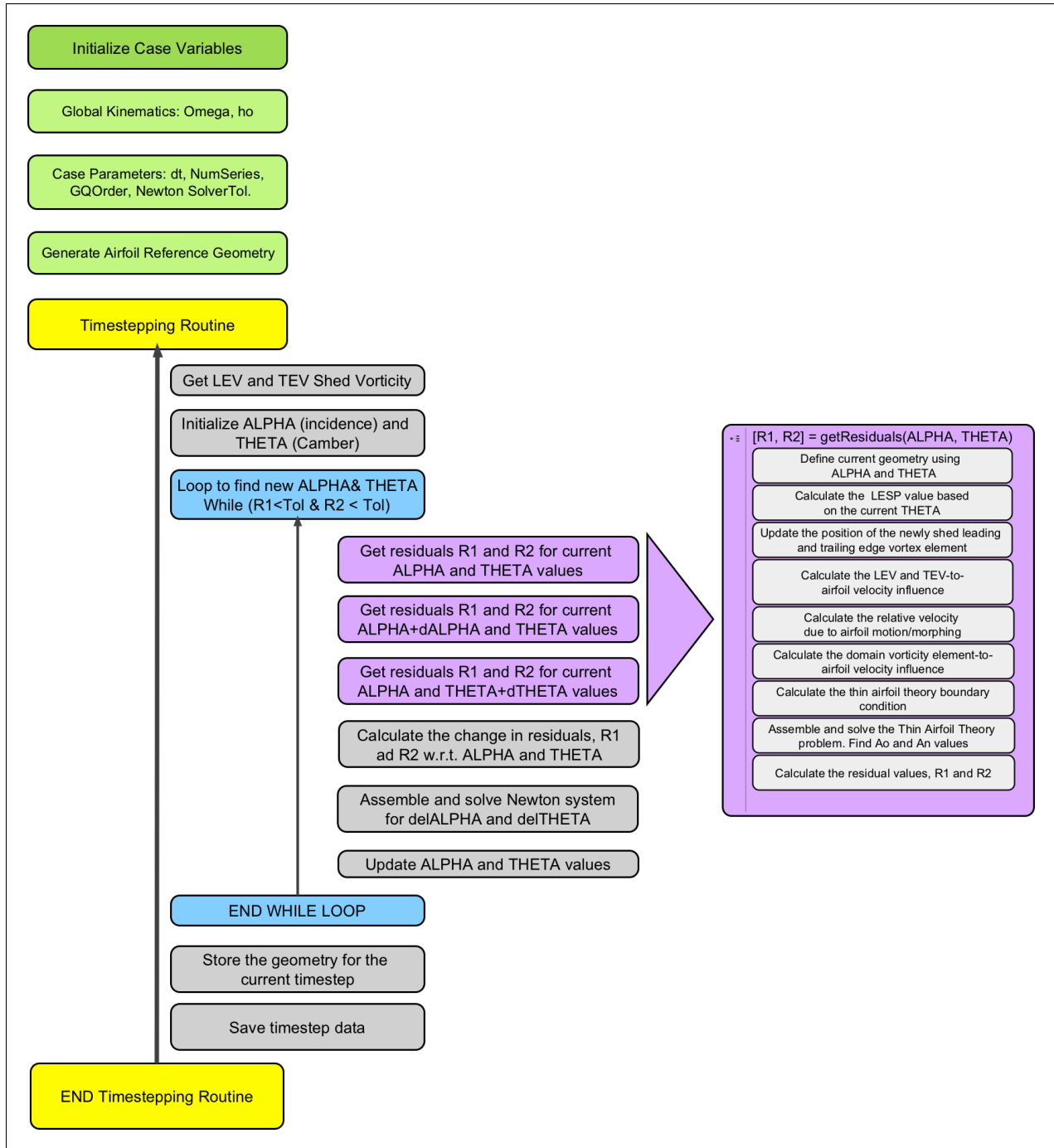


Figure 5. Pseudo code illustrating the inverse design process using the thin-airfoil-theory method, including the LESP criteria.

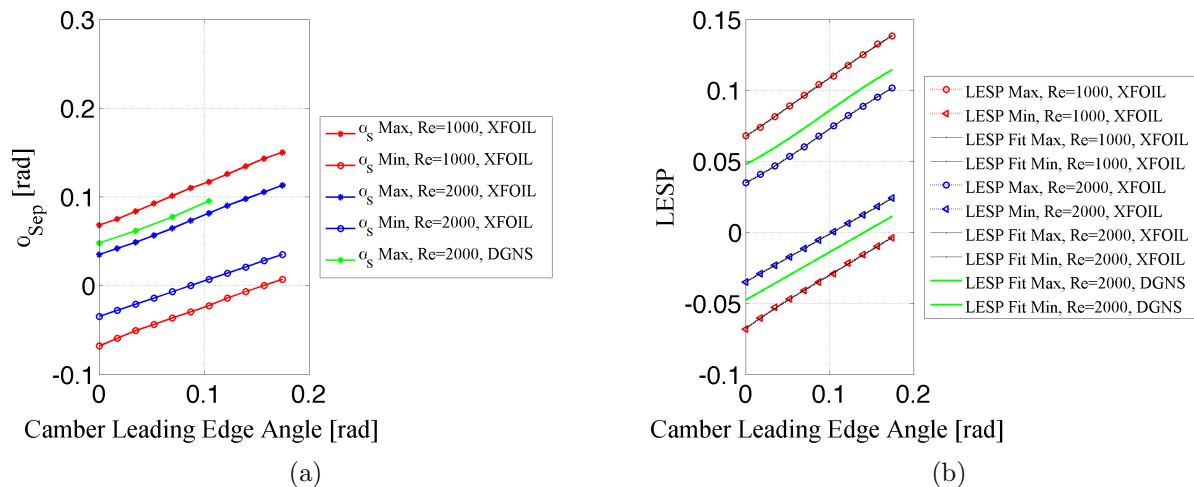


Figure 6. (a) The critical angle of attack where leading edge separation first occurs in a static airfoil case as a function of camber angle for Reynolds number 1,000 and Reynolds number 2,000 using XFOIL and CFD. (b) The value of the leading edge suction parameter derived from the results of the CFD and XFOIL calculations. In addition, a cubic fit of the data is applied to determine an approximate functional relationship between camber and LESP.

III.A.5. Two-Dimensional Navier-Stokes

For the high-fidelity simulations, we use a high-order accurate discontinuous Galerkin method (DG) method based on unstructured simplex mesh elements and nodal basis functions.²¹ High order methods are advantageous for applications requiring low numerical dispersion and high time accuracy. The DG method produces stable discretizations of the convective operator for any order discretization, thus avoiding the need for additional stabilization or filtering. Here, we use nodal basis and polynomial orders $p = 3$. The viscous terms are discretized using the Compact Discontinuous Galerkin (CDG) method, the deforming domain is handled with a mapping-based Arbitrary Lagrangian-Eulerian (ALE) scheme, and implicit Runge-Kutta schemes are used for the time integration. The nonlinear system of equations that arise from the discretization are solved with a Newton-Krylov method and a block-ILU(0) preconditioner.

The ALE formulation requires that the deformations are prescribed either explicitly or indirectly as a mapping $x = x(X, t)$ between the reference and the physical space. Here, we compute these mappings numerically from the corresponding deformed meshes, which are produced by solving a nonlinear elasticity problem that smoothly deforms the mesh elements according to the deformed boundaries. An example is shown in figure 2. Subplot (d) shows the reference geometry and the corresponding mesh, which has zero degree camber and angle of attach. Subplots (e) and (f) show the deformed meshes for $\theta = 5$ and $\theta = 15$. These are used to evaluate the deformation gradients $\partial x / \partial X$ and the grid velocities $\partial x / \partial t$ used in the ALE formulation.

III.B. Three-Dimensional Geometry Definition & Computational Methods

We take a similar approach in three-dimensions as we did in two-dimensions, starting first with a wake-only method,^{24,29} followed by a quasi-inverse design³⁰⁻³² and finally a three-dimensional Navier-Stokes simulation.³³ In three-dimensions, the analysis becomes a little more involved due to the increased number of degrees of freedom.

III.B.1. Three-Dimensional Geometry Definition²⁹

The first step in determining the flapping wing geometry is to prescribe a wing planform (see Figure 7 for the wing geometry definition). We currently use a second order, parametric polynomial to define both the leading and trailing edge planform shape. For the cases that will be presented in this paper, we prescribe the wing camber and modulate the wing twist. The wing section camber is defined using a Hermite cubic spline, in a manner analogous to the two-dimensional cases presented in section III.A.1.

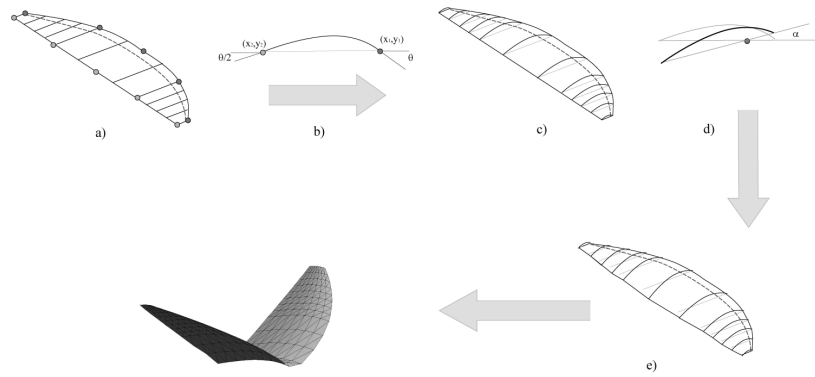


Figure 7. The wing geometry definition in the QI-DLM method starts with a planform definition. The camber along the span is then prescribed. Following this, the twist angle is imposed and the wing is rotated through the flapping angle.

III.B.2. Three-Dimensional Wake-Only Method^{24, 29}

Our wake-energetics code^{24, 29} was used to determine the wake shape, the wake shed vorticity distribution, and the wing global kinematics. Our energetics prediction method first generates a large database of wake-only solutions for the different wing kinematics (*offline module*). For each wake shape and lift/thrust coefficient pair, the optimal circulation distribution is evaluated and stored. An *intermediate module* distills the *offline database* into a series of multi-dimensional response surfaces for each flight velocity in the vehicle's flight envelope. For each velocity, only one unique combination of the flapping kinematics and wake-circulation distribution can satisfy the flight force constraint (lift equals weight, drag equals thrust). To determine this unique operating point for each different combination of flapping kinematics, a non-linear solution is performed. The result is a collection of wake-only predictions that satisfy the flight constraints using different flapping kinematics at each flight speed considered (i.e. for each flight velocity, there is a single wake circulation, and power requirement corresponding to each combination of the flapping kinematics). The *online module* takes these viable *intermediate flight results* and distills them further into the collection of optimal wakes for the flight velocity being considered. This energetics framework can provide efficient wake shapes and circulation distributions in a design context at a fraction of the price of a high fidelity analysis.

III.B.3. Three-Dimensional Quasi-Inverse Wing Design

We have developed a quasi-inverse doublet lattice method tool for determining flapping wing shapes using wake-shapes and wake-circulation distributions.³⁰⁻³² In the potential flow setting there are an infinite number of wing geometries that can produce the desired wake-circulation distribution; however, only a small handful of these geometries might actually be successful in a real fluid. By modulating the wing camber and twist angle together, we can produce viable wing geometries.³²

Once a flapping wing twist-camber strategy is selected, we use a quasi-inverse doublet lattice method to determine the wing shape. In the cases presented in this paper, the QI-DLM is used to determine the local wing twist angle in order to achieve the desired trailing wake vorticity/circulation distribution. This twist distribution is modulated at each step of the inverse design process to find the flying wing shape that matches the desired shed wake.

III.B.4. Three-Dimensional Navier Stokes

For our high-fidelity verification simulations, we use the same discontinuous Galerkin techniques as described above for the 2D case. The main difference is that our 3D simulations require fully unstructured tetrahedra meshes, which we generate using a combination of the DistMesh method and the Delaunay refinement method. Also, the problems are too large for solving on a single CPU, and we use the parallel capabilities of our *3DG* code²¹ to solve on between 192 - 768 CPU cores with a domain decomposition based technique.

The code and the method has been used and tested extensively for simulation of wing designs similar to those being examined in this research.³²

IV. Wing Design Studies, Results and Discussion

We present three different studies that illustrate the capability of our computational tools:

1. **Pitch-Ramp Study:** This study examines how the LEV on a simple pitch-ramp motion can be modulated by simultaneously varying the pitch angle and camber (leading edge angle), to achieve a desired vorticity shedding rate at the leading and trailing edges.
2. **2D Heave Downstroke Study:** This study examines the downstroke-half of the flapping cycle and attempts to shed a reasonable strength vorticity distribution from the leading edge. The goal here is to shed into the domain the optimal vorticity distribution for a range of thrust coefficients: $C_T = 0.25, 0.50$ and 0.75 .
3. **3D Flapping Study:** This study preliminarily examines how span-wise variation of the leading edge angle can affect the flow around an quasi-optimal designed three-dimensional wing.

The studies also provide some preliminary insight into how LEV formation and evolution can be modulated using camber and wing incidence variations. While preliminary, these studies show the promise of tailoring LEVs for low-Reynolds number applications.

IV.A. Preliminary Two-Dimensional Pitch-Ramp Studies

In this first example, a series of cases are run to modify the shed vorticity from a simple pitch-ramp maneuver of a zero-camber wing. The goals of this experiment were:

1. To validate the operation of the inverse design tool by demonstrating that the original zero-cambered, pitching airfoil baseline case could be recovered using only the target leading and trailing edge shed wake from that baseline case in a quasi-inverse design process.
2. To qualitatively confirm the results of the thin-airfoil theory for inverse design applications. This includes the ability to modulate the formation and evolution of the LEV on pitching wings.
3. To examine how a reduction in leading vorticity shedding impacts the development and persistence of the LEV.
4. To examine how the camber and thus leading edge angle is modulated to achieve lower or zero-vorticity shedding at the leading edge.

IV.A.1. Description of the cases

A baseline case (Case 0) along with twelve design cases (Case 1 through Case 12) are presented in this section. In each case, the leading and trailing edge shed vorticity from the baseline is manipulated to explore the development of the LEV:

- **Case 0:** A simple pitch-ramp simulation of prescribed motion kinematics. In this case, the airfoil has zero-camber, and the pitch angle is defined using the following function:¹⁷

$$\beta(t) = \ln \left(\frac{\cosh(a(t - t_1)) \cdot \cosh(a(t - t_4))}{\cosh(a(t - t_2)) \cdot \cosh(a(t - t_3))} \right) \quad (5)$$

$$\alpha(t) = \frac{\hat{\alpha}\beta}{\max(\beta)} \quad (6)$$

where, $t_1 = 1$, $t_2 = t_1 + \frac{1}{2\pi f}$, $t_3 = t_2 + \frac{1}{2f} - \frac{1}{\pi f}$, and $t_4 = t_3 + \frac{1}{2\pi f}$. In this case, $a = 2$, $K = \frac{\omega}{2} = 0.11$, and $\hat{\alpha} = 20^\circ$. For simplicity, we consider time $0 < t^* < 6$.

- **Case 1, Validating the quasi-inverse design methodology:** This case is a validation case to illustrate that our inverse design framework can regenerate the wing and wing motion based on the shed trailing and leading edge vorticity. In this case the shed leading and trailing edge vorticity from case 0 are prescribed as inputs to the airfoil inverse design tool with the goal of recovering the pitch angle and camber prescribed in case 0 . The case is run from $0 < t^* < 4$.
- **Case 2 - Case 5, Manipulating the LEV Shedding Rate:** In these cases, we prescribe the same shed vorticity from the trailing edge of the airfoil as in Case 0, but we prescribe a fractionally lower leading edge vorticity shedding rate than that in Case 0. The intent of these cases, is to observe how the evolution of the LEV is affected when the baseline shedding rate is decreased by a certain percentage. In addition, we are interested to observe how the kinematics and camber change as a function of time to allow the airfoil to achieve this desired shedding rate.
 - **Case 2:** Leading edge shedding rate 95% of that observed in Case 0.
 - **Case 3:** Leading edge shedding rate 90% of that observed in Case 0.
 - **Case 4:** Leading edge shedding rate 75% of that observed in Case 0.
 - **Case 5:** Leading edge shedding rate 50% of that observed in Case 0.
- **Case 6 - Case 10, Manipulating the Wing Bound Circulation:** In these cases, we maintain the same trailing edge shedding rate as that observed in the baseline case (Case 0), however, we control the change in circulation associated with the wing. In this case, the LEV still changes strength to satisfy Kelvin’s Circulation theorem. The goal of these studies was to examine whether there was a relationship between the wing vorticity contribution and the development of the LEV:
 - **Case 6:** The wing bound circulation is set to 75% of the Case 0 value.
 - **Case 7:** The wing bound circulation is set to 50% of the Case 0 value.
 - **Case 8:** The wing bound circulation is set to 25% of the Case 0 value.
 - **Case 9:** The wing bound circulation is set to 0% of the Case 0 value.
 - **Case 10:** The wing bound circulation is set to –25% of the Case 0 value.
- **Case 11 - Case 12, Eliminating LEV Shedding:** In these two cases, we apply the quasi-inverse design tool to determine the dynamic wing shape that results in zero shedding from the leading edge, yet maintains the same trailing edge shedding rate.
 - **Case 11:** For this case, the leading edge shedding rate is set to zero, and an LESP is prescribed according to: $LESP_{presc.} = 0.75LESPMax_{case0}$.
 - **Case 12:** For this case, the leading edge shedding rate is set to zero, and an LESP is prescribed according to: $LESP_{presc.} = 0.9LESPMax_{case0}$.

IV.A.2. Validation of the Inverse Design Approach, Comparing Case 0 and Case 1

First we compare Case 0 and Case 1 to confirm that the inverse design methodology is capable of recovering the baseline wing camber and pitch angle using only the time signature of the vorticity shed from the leading and trailing edges.

Figures 8, (a)-(c) show the time history of the total circulation (shed from the leading and trailing edges, as well as the net bound circulation on the airfoil), the pitch angle and camber, and the leading edge suction parameter for the case as computed using the evaluation mode of the thin airfoil theory approach. Figures 8, (d)-(f) illustrate the same quantities from the quasi-inverse design mode of the thin airfoil theory method. Comparing the originally prescribed pitch angle and camber in figures 8, (b)-(c) with the outputs of the design code in figures 8, (e)-(f) shows good agreement, demonstrating that the quasi-inverse design process is capable of recovering the original wing kinematics. This result indicates that our quasi-inverse design methodology is able to recover the original airfoil shape and kinematics using only the vorticity shed from the leading and trailing edges.

In this baseline case, the evolution of the bound circulation on the airfoil as well as the total circulation in the leading and trailing edge vorticity distributions exhibit interesting behaviors. At the beginning of the

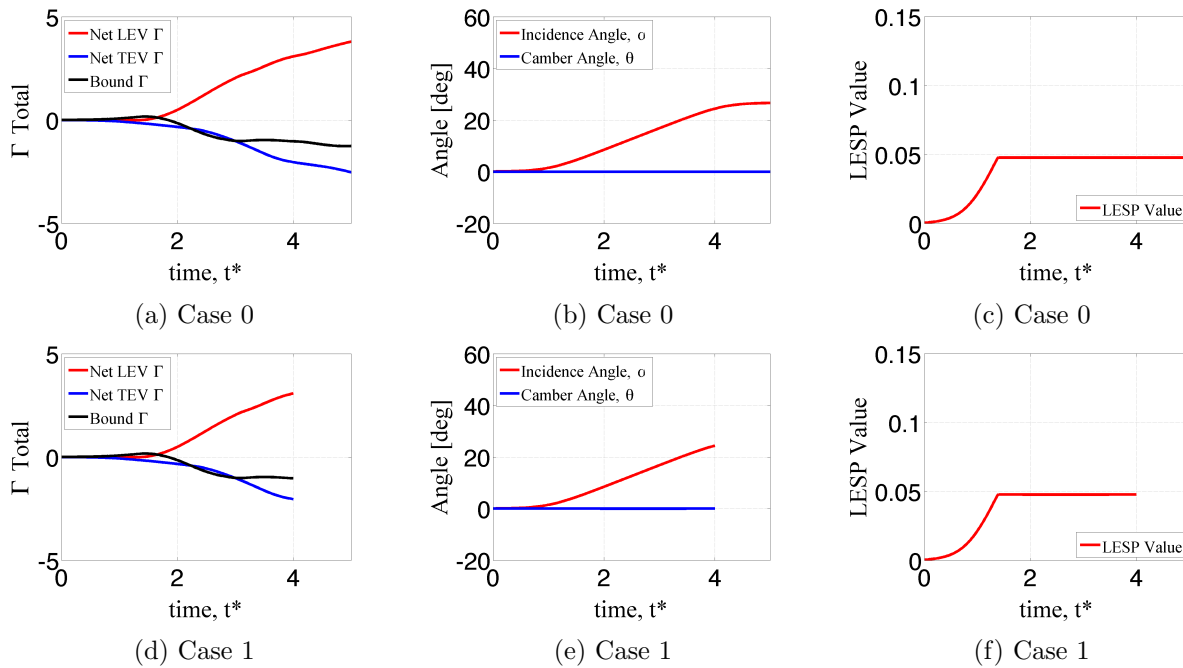


Figure 8. Comparison of the baseline case (Case 0) and the quasi-inverse design to recover the baseline (Case 1). The baseline case follows a pitch-ramp motion of a flat plate, during which leading edge vorticity shedding forms a LEV structure above the wing. The Case 1 results show good agreement with the baseline and indicate that the quasi-inverse design method can successfully recover the original wing shape from only the leading and trailing edge shedding rates.

pitch-ramp motion, the wing bound circulation increases to match the shed trailing edge vorticity – since no leading edge vorticity shedding is present. This represents the traditional aerodynamic behavior, where a wing bound circulation is developed resulting in a lift force. After approximately $t^* = 1.5$, the LESP reaches a critical value and leading edge vorticity shedding begins to occur. As vorticity is shed at the leading edge, the circulation associated with the wing vorticity distribution (wing bound vorticity) decreases and becomes negative valued as the leading edge vortex rapidly grows in size and strength. It appears that the bound circulation associated with the wing is the primary balance for the leading edge vortex circulation growth and the trailing edge vorticity shedding. As time progresses, the bound circulation and the circulation shed into the trailing wake are similarly valued (both negative), resulting in a leading edge vortex with nearly double the strength of either the bound and trailing edge shed circulation. This result is particularly interesting since it suggests a significant kinetic energy expenditure to develop and grow the leading edge vortex in this case.

The leading edge vortex is traditionally associated with augmented circulatory force production. In effect, the LEV acts to increase the bound vorticity associated with the wing. While the leading edge vortex is the dominant circulatory lift force production mechanism, the negative circulation associated with the wing vorticity distribution counteracts some of the circulatory effect of the LEV. In this case, it appears that some of the energetic expense of generating an LEV is devoted to counteracting the wing bound vorticity system, and not solely devoted to generating augmented forces. In the remaining cases, we will explore this circulation balance further.

Figure 9 a-h provide a visual comparison between the baseline computation and the quasi-inverse design of the same problem. In both cases, the flow around the airfoil shape and kinematics were simulated using high order CFD. This comparison between the CFD and the LESP augmented thin airfoil theory approach illustrates that the thin airfoil theory model has good visual agreement between the evaluation and the quasi-inverse design modes. Additionally, the results indicate that the CFD simulations and the thin airfoil theory exhibit a similar flowfield. This is a good indication that our lower-fidelity models (like those of Gopalarathnam et al.²⁵⁻²⁷) have a decent analysis capacity in both design and flow evaluation for these leading edge separated flows.

Figure 10 a-b illustrates the force coefficient generation history (using CFD) for the pitch ramp motions.

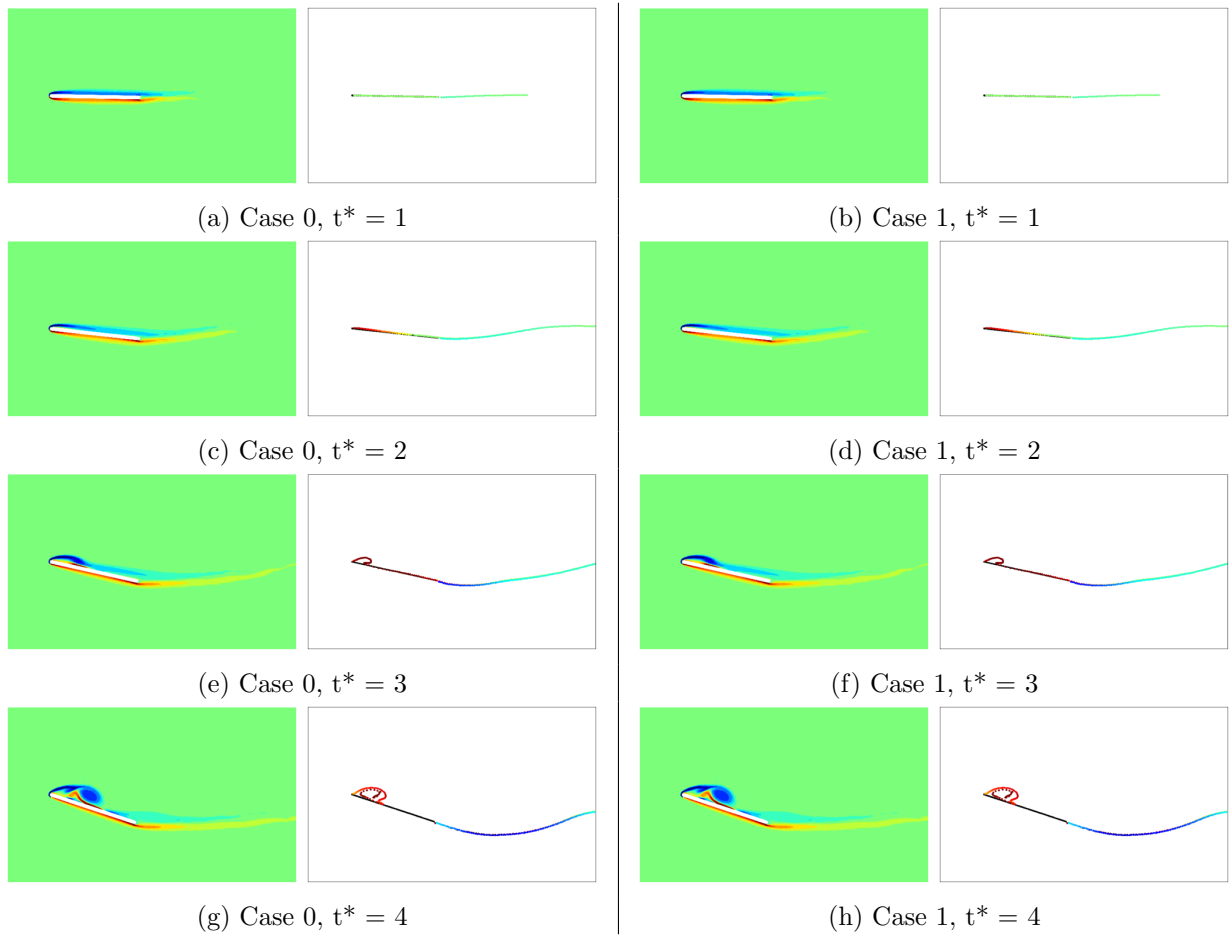


Figure 9. A comparison between the baseline simulation (left column) and the quasi-inverse simulation (right column).

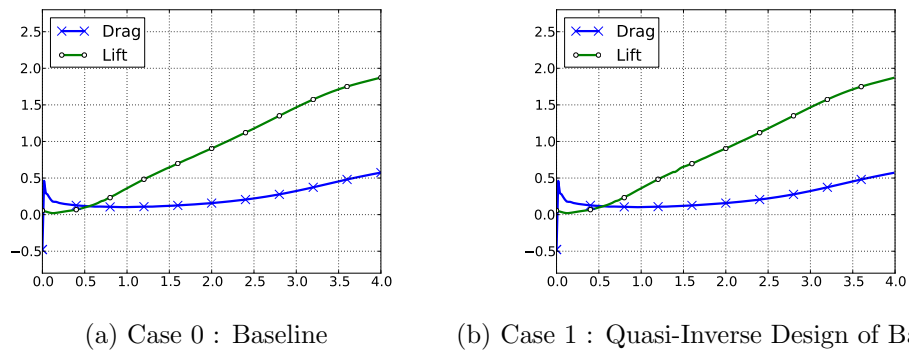


Figure 10. The CFD computed force coefficients for Case 0 and Case 1 with respect to non-dimensional time.

In both the direct and quasi-inverse design results, the forces are effectively the same, again confirming the inverse design method's operation. The lift coefficient gradually increases throughout the maneuver, while the drag forces initially are reduced, but increase as the case progresses. In both cases the force evolution is smooth, indicating that the kinematics as well as the airfoil shape change are gradual. In addition, the smooth time-history of the forces is indicative of a LEV that remains attached through the time period considered.

IV.A.3. Cases 2-5: Manipulating the Leading Edge Shedding Rate

In this section, we examine the impact of reducing the LEV strength by different fractional amounts by manipulating the LEV shedding rate. In these cases, the LEV shedding rate from the baseline case is scaled by different amounts while maintaining the trailing edge shedding rate. The trailing edge shedding rate is maintained, since it represents the combination of the wing and LEV circulations – and therefore, in essence the total bound circulation (here we assume that an attached LEV combined with the wing bound circulation represents the total bound circulation associated with the wing). By maintaining the same TE shed vorticity and the same total wing bound circulation, we implicitly maintain similar circulatory forces for the different cases – a valuable similarity for comparisons.

In cases 2-5 the shedding rate at the leading edge is reduced to 95%, 90%, 75% and 50% of the baseline case 0 value respectively (Figure 11 - 13). The goal of this study was to examine how this reduction in LEV strength impacts the generation and evolution of the LEV, when the same trailing edge vorticity shedding rate was imposed.

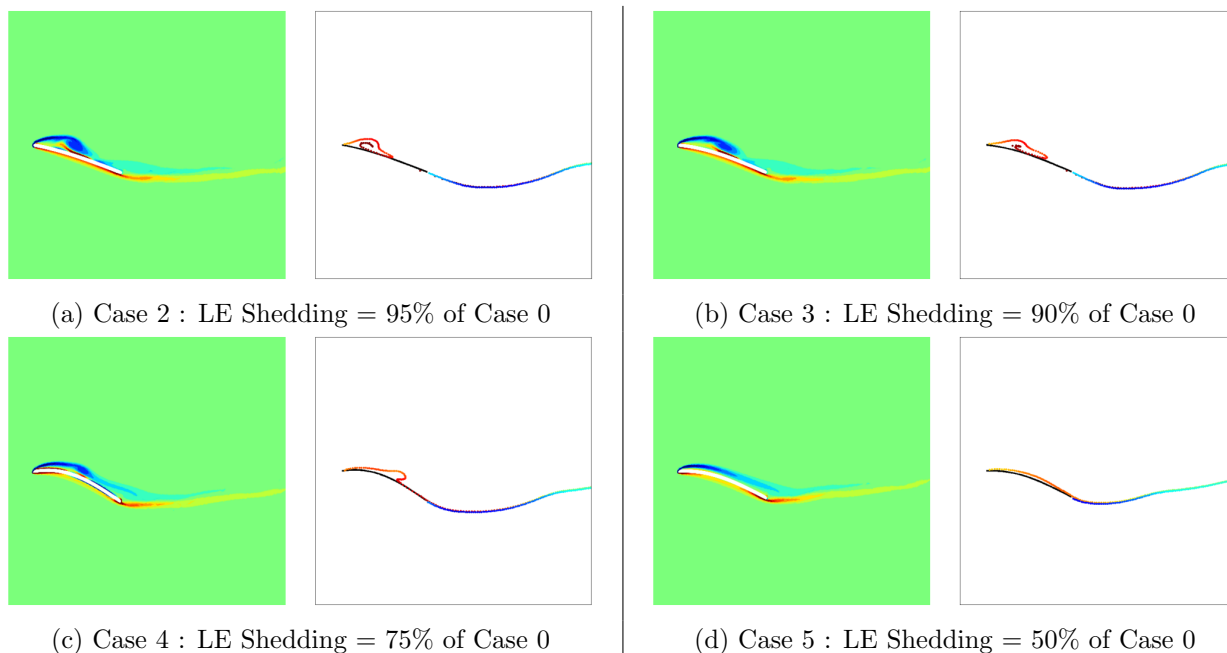


Figure 11. The CFD and thin airfoil theory results for the final timestep of the flow simulation for cases with reduced prescribed leading edge shedding (Cases 2-5).

Figures 11 a-d illustrate the final time-step of the reduced LE shedding strength thin airfoil theory inverse design predictions and CFD simulations. Compared with the baseline (Figure 9), the LEV development is visually different, even when the LE shedding rate is reduced only by 5% or 10% (cases 2-3). When the LE shedding rate is reduced by 25% the LEV that is formed is substantially smaller and has propagated further downstream than in the previous cases. When the LE shedding rate is reduced by 50%, a coherent LEV structure does not form, resulting simply in LE shedding. These results suggest that the LE shedding rate does impact the development and evolution of the LEV.

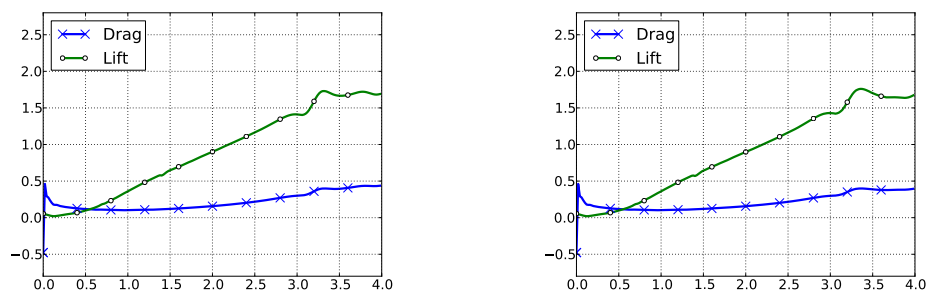
Figures 12 a-d illustrate the time evolution of the lift and drag force coefficients simulated using CFD when the LE shedding rate is reduced. Despite the significant reductions in leading edge shedding rate, the time history of the force coefficients is very similar between the cases. In particular, during the initial three

time units, the ramp in the lift coefficient is nearly identical to the baseline in all cases (Figure 10). In cases 4 & 5, the force evolution is similar until the force coefficient reaches a value of 1.6, and the force can not be sustained any longer.

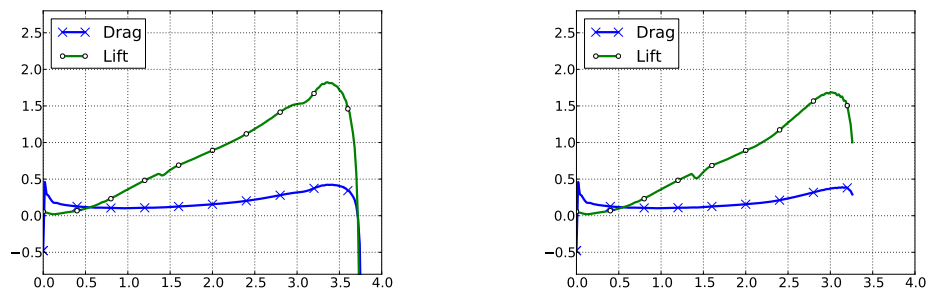
The force coefficient results suggest several considerations when using LEVs to augment force production:

- Below a certain force coefficient value, the presence of an LEV does not add any benefit in the force production capability. In the cases shown, it appears that the LEV is only beneficial when the force coefficient is greater than 1.6 in value.
- The attached LEV structure acts in a manner similar to wing bound vorticity. This implies that an attached LEV acts as the circulation required to turn the flow, much like the bound circulation on a cambered airfoil.
- The trailing edge shedding rate is one of the primary determinants of the circulatory force production. If the TE shedding rate is similar, one can balance wing vorticity and LEV circulation to achieve the desired total bound circulation at the wing.

From this set of cases, the balance of circulation between the LEV and the wing bound vorticity distribution appears to be somewhat interchangeable (at least for lower force coefficient values).



(a) Case 2 : LE Shedding = 95% of Case 0 (b) Case 3 : LE Shedding = 90% of Case 0



(c) Case 4 : LE Shedding = 75% of Case 0 (d) Case 5 : LE Shedding = 50% of Case 0

Figure 12. The CFD computed force coefficients for Case 0 and Case 1 with respect to non-dimensional time.

Figures 13 a-l illustrate the time evolution of the various vorticity shedding rates, the camber and incidence angle and the LESP value. The plots showing the time evolution of the circulation contributions (Figures 13 a,d, g,& j) for each case illustrate how the reduction in the LE shedding rate also impacts the wing bound vorticity. As the LE shedding rate is reduced, the bound circulation increases – to a point in Case 5 where the wing bound circulation remains positive throughout much of the time examined.

Figures 13 b,e,h, & i illustrate how airfoil camber and incidence angle are increased over time to reduce the rate of shedding from the leading edge - with lower prescribed LE shedding rates, the airfoil leading edge must align more with the flow, resulting also in the need for higher incidence angles to turn the flow and match the TE shedding rate. This increased camber angle also produces a higher critical LESP value, which also reduces the LE shedding rate. The results suggest that the combined effect of leading edge flow alignment and the increased LESP value are together responsible for lowering the leading edge shedding

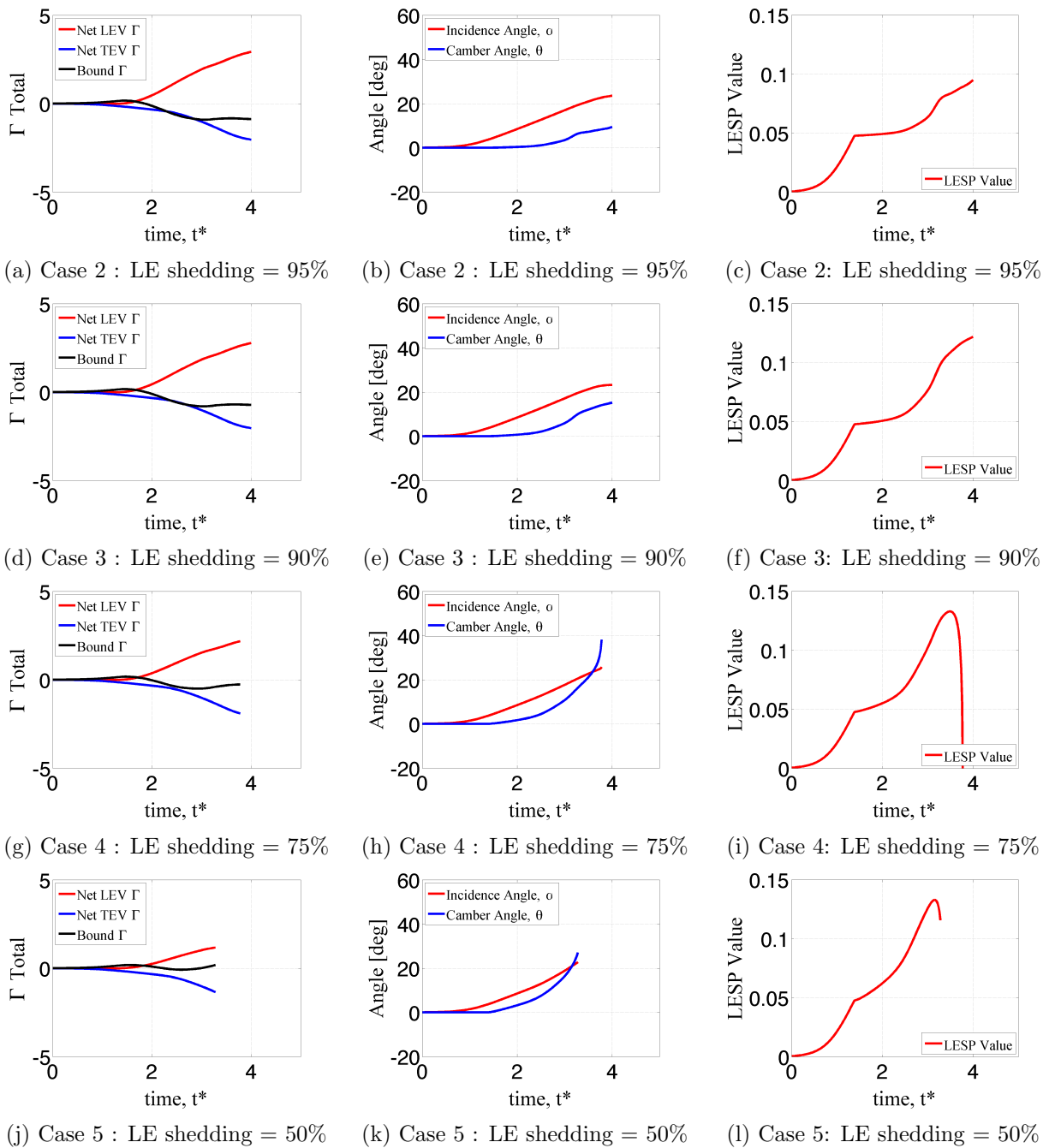


Figure 13. The thin airfoil theory quasi-inverse design method results for cases 2-5.

rate. The evolution of the airfoil camber in time is consistent with expectations and suggests that LEVs can have a similar effect on the flow as airfoil camber. To maintain a similar trailing edge shedding rate as our baseline, Case 0, the incidence angle of the airfoil must also increase.

The results of the investigation modulating the leading edge shedding rate confirm the hypothesis that formation of a leading edge vortex structure is strongly dependent on the leading edge shedding rate. Examining the results in figures 13: g-l closely, illustrates several changes have occurred in the evolution of the bound circulation and the airfoil shape. First, the wing bound circulation is close to zero in these final two cases; whereas, in earlier cases where an LEV was seen to be dominant, the wing bound circulation had a significant negative value. In addition, in these cases, the camber angle θ is relatively large, exceeding 20 degrees toward the end of the maneuver. This highly cambered airfoil configuration is (a) more aligned with the local freestream and (b) is likely to have a less aggressive pressure peak at the airfoil leading edge and it is therefore unlikely to be conducive for generating an LEV structure. Finally, because the prescribed LEV shedding rate is lower, the LEV circulation is also lower, and the ability to generate a flow reversing LEV structure on top of the airfoil is compromised.

While further study into the limits of LEV formation is required, the results of the quasi-inverse approach suggest the following:

1. The strength of the LEV is dependent on the vorticity shedding rate at the leading edge.
2. The formation of the LEV appears to be linked to a negative wing-bound circulation.
3. Camber and incidence may be used to mitigate LEV development while maintaining identical trailing edge shedding properties.

The ability to modulate the shedding rate has made these preliminary observations possible. While the traditional approaches (modeling prescribed wing shapes and kinematics) support these conclusions, the traditional approach is more ad-hoc and passive in forming these conclusions as the wing and kinematics variations considered are not being directly driven by shedding rate considerations.

IV.A.4. Cases 6 - 10: Manipulating the Wing Bound Circulation

It was observed in Cases 1-5 that a leading edge vortex appeared to form only when the wing bound circulation was below zero for a sustained period of time. To further examine the effect of the wing-bound circulation on the formation and evolution of LEVs, we performed Cases 6-10 to examine how modulating the wing bound vorticity directly affected the development of the LEV. These cases were examined to test whether the formation of an LEV was impacted by the value of the circulation associated with the wing.

The results in figures 15, once again show that leading edge angle or camber increases significantly as the prescribed LE shedding strength is reduced – again increasing alignment between the leading edge and the flow. The plots also illustrate how the wing bound circulation approaches a near zero value in some of the cases.

The results presented in figure 14 a-e illustrate how reductions in the the value of the wing bound circulation has an impact on the LEV structure formation. In particular, the LEV forms a coherent structure when the wing bound circulation is significantly less than zero for extended periods of time (Case 6 and 7). Conversely, when the bound circulation has a zero- or positive value, the LEV does not form a coherent structure as can be seen for cases 9 and 10 (figure 14-d-e). Case 8 illustrates the simulation results for the case where the wing bound circulation is 25% of the original baseline value. In this case, there is a separated flow with re-attachment, but further investigation would be required to ascertain that an LEV structure is formed. This further supports the earlier conclusion that wing bound circulation must have a substantially negative value to reverse the flow and generate an LEV. This result is interesting, in that it suggests that the circulation contribution from the wing opposes that of the LEV when the LEV is coherent. This result suggests that the LEV structure generates an excess of circulation to generate the desired lift augmentation. Whether this result carries into three dimensions has yet to be explored.

IV.A.5. Cases 11 and 12: Eliminating the Leading Edge Shedding

By its nature, the quasi-inverse design methodology also permits the design of airfoils that will have zero or minimal leading edge shedding. In addition to the prescribed vorticity shedding, we also prescribe a leading edge suction parameter (LESP) value below the critical value. As a result, an airfoil shape and

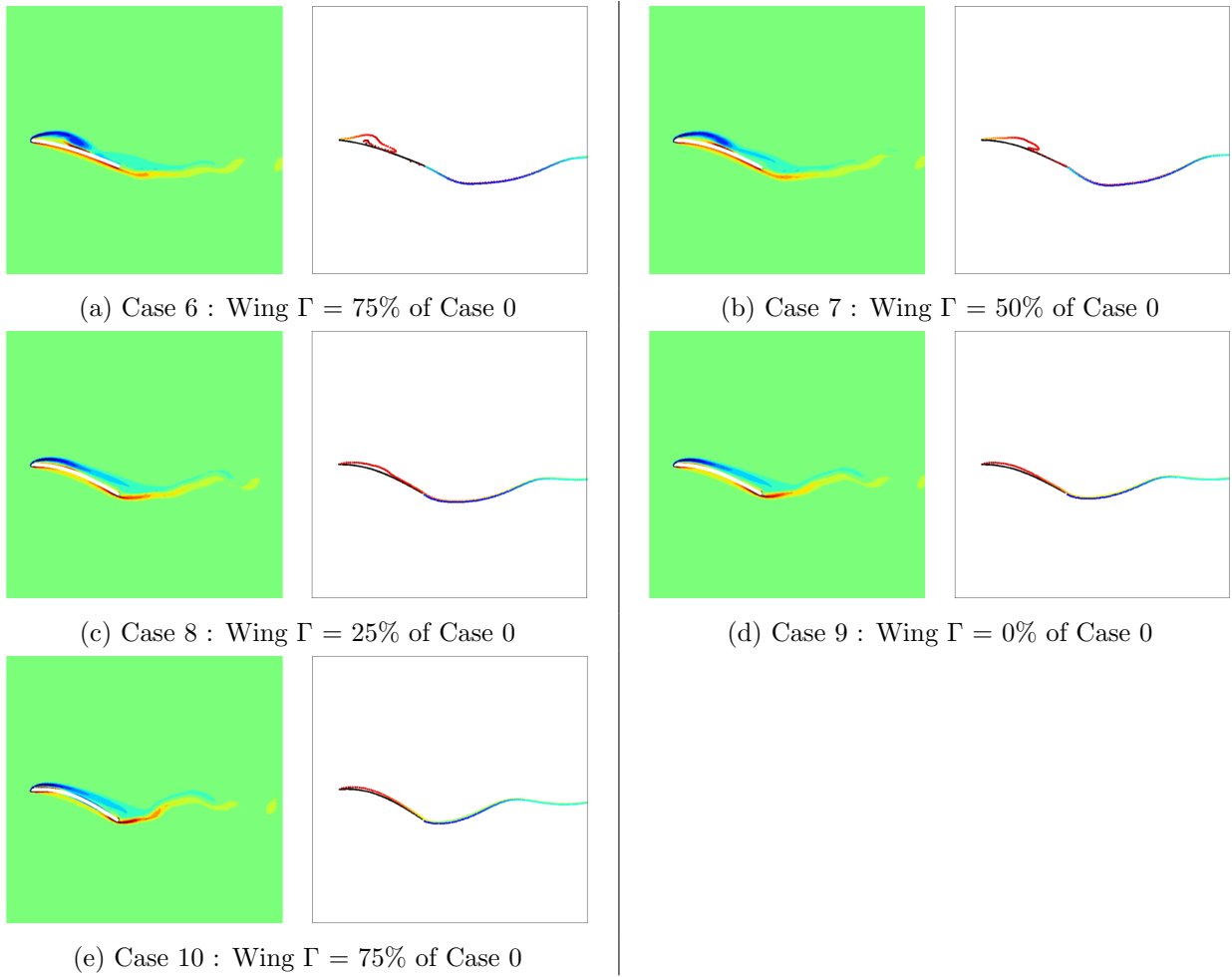


Figure 14. The CFD and thin airfoil theory results for the final timestep of the flow simulation for cases with reduced prescribed leading edge shedding (Cases 6-10).

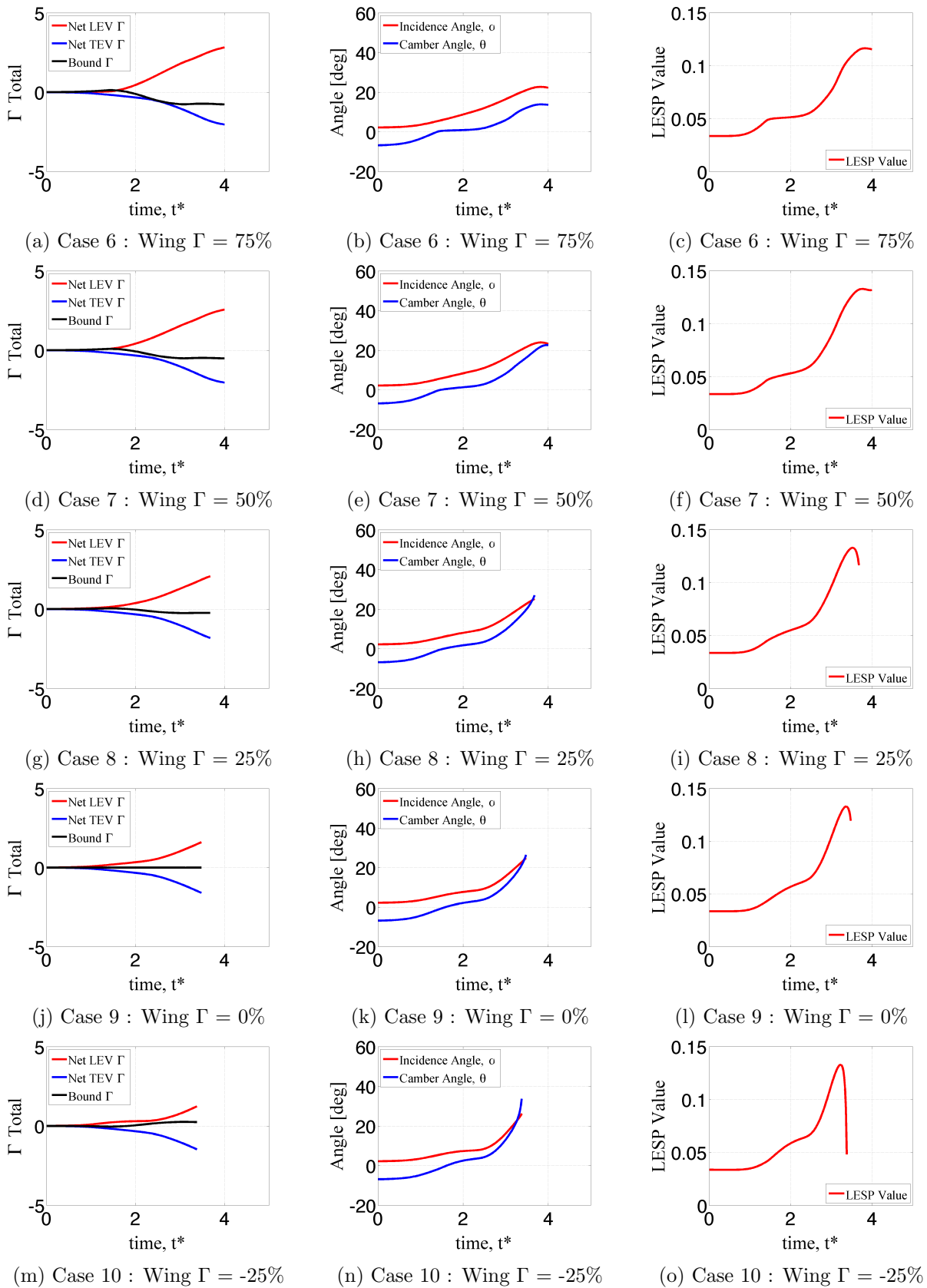


Figure 15. The thin airfoil theory quasi-inverse design method results for cases 2-5.

incidence is determined that prevents vorticity shedding at the leading edge, but still maintains the trailing edge shedding rate. We examined a pair of preliminary cases (Cases 11 and 12) in which the airfoils were designed to minimize leading edge shedding altogether. Figures 16 & 17 show the results of this study.

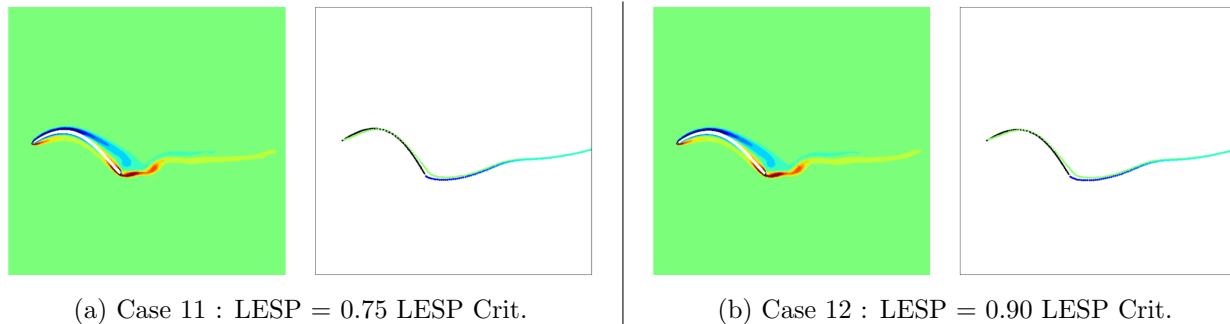


Figure 16. Thin airfoil theory and CFD simulations of the flow around the airfoils for cases where shedding is mitigated (cases 11 and 12).

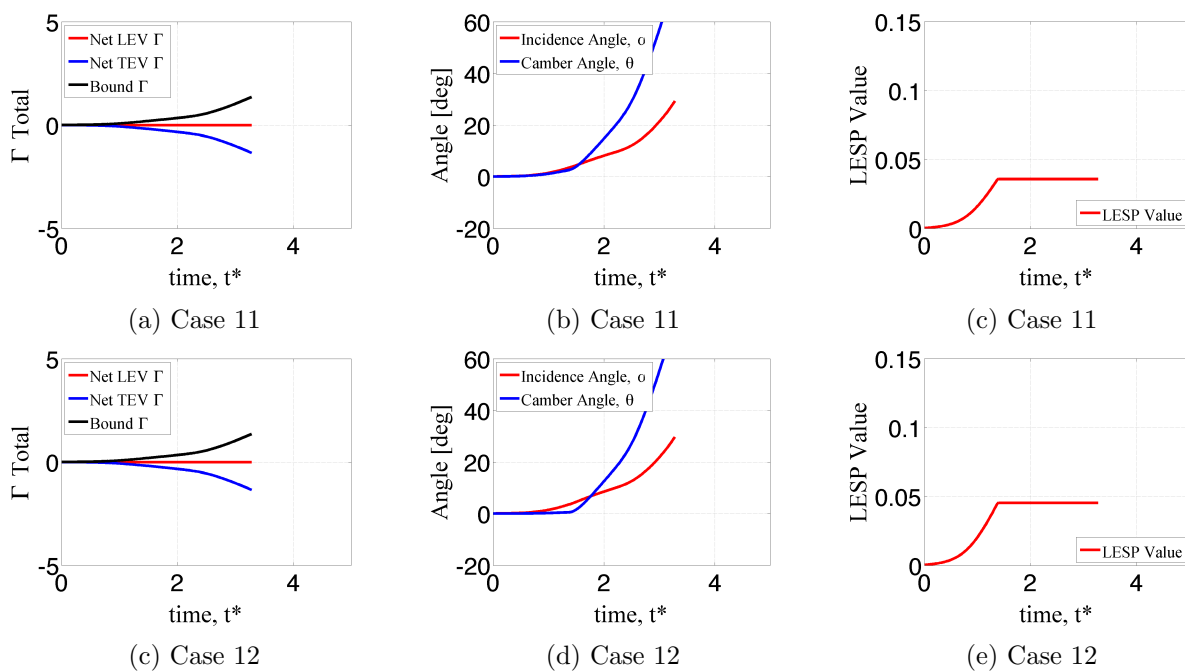


Figure 17. The thin airfoil theory quasi-inverse design method results for cases 7 and 8.

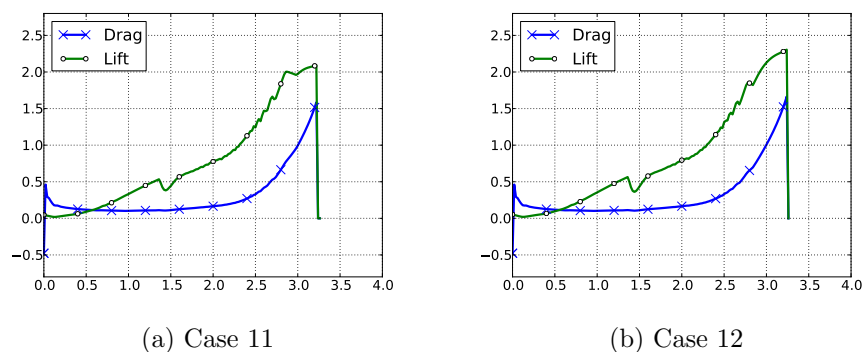


Figure 18. The CFD computed force coefficients for Case 0 and Case 1 with respect to non-dimensional time.

In order to mitigate vortex shedding from the leading edge while maintaining aggressive trailing edge shedding rates, the airfoil must be highly cambered. In figures 17, b & d, we observe that the airfoil camber is significant, reaching in excess of $\theta = 50$ degrees. In figures 16, the CFD and thin-airfoil theory results show good agreement, even with a highly cambered airfoil.

The force coefficient history when no leading edge shedding is prescribed is similar to the baseline case, however, several notable differences exist. First, the increase in the force production as a function of time is slightly less linear, and is also more aggressive than the baseline as time evolves. This is likely due to the dynamic cambering effect that augments the unsteady force production at later stages of the maneuver. In addition, the drag force coefficient is initially similar, but rapidly increases towards the end of the simulations. This is likely due to trailing edge separation effects that undoubtedly are initiated at the high camber, high incidence end condition that is required to mitigate leading edge shedding. Overall, however, it is surprising that the lift force is similar in maximum magnitude as the baseline despite the absence of an LEV. This suggests that the presence of an LEV may be at times, replaced with a highly cambered airfoil with a high bound vorticity/circulation. While this may not apply for very high lift settings, the present study suggests that the presence and effect of an LEV may be achieved with a dynamically cambered airfoil at a lower energetic cost. This result suggests that animals such as birds and bats, that do use active cambering wings may have some ability to control when an LEV forms and when wing cambering may be a more appropriate solution.

IV.B. Preliminary Two-Dimensional Half-Flapping-Cycle Wing Studies

In this section we describe a series of heave-pitch cases that mimic the downstroke of a flapping cycle. This is achieved by considering a leading edge vertical heaving motion defined as:

$$h(t) = h_o \cos(\omega t), \quad (7)$$

based on the results of the wake only method solutions ($h_o = 1.25$, $\omega = \omega_{optimal}$). In this series of examples, only half of a cycle of the above motion is examined. In order to maintain an efficient thrust generation, we aim to produce the vorticity in the domain as prescribed by the wake-only method. There are several strategies that could be used, however, for this initial study of flapping motions, we were only able to study the case where the trailing edge vorticity was set to match the wake-only target vorticity distribution and the leading edge vorticity shedding was set to zero. The results of the quasi-inverse design are presented in figure 19.

The half-flapping-cycle results in figure 19- b,e, & h show the variation of the camber and incidence angle when an attempt is made to mitigate leading edge vorticity shedding. In these cases, the pitch angle of the airfoil remains similar, however, the camber becomes increasingly more aggressive with increases in thrust coefficient. This is consistent with the flapping frequency, which tends to increase with desired thrust.

The results for the camber and LESP as a function of time both exhibit a slope discontinuity at the mid-flapping cycle (figure 19). This corresponds to the implementation of the LESP condition in our quasi-inverse design code. The LESP value was set to 95% of the critical value, with a similar sign as the shed trailing vorticity. At mid-downstroke/heave, the trailing edge shed vorticity transitions from a positive to a negative value. This rapid change in the prescribed LESP results in a similar rapid change of the camber angle. In future studies, a more careful prescription of the LESP value will be undertaken.

The visualization of the flowfield for the downstroke motions can be seen in figures 20: a-c. The CFD results exhibit a history of shedding in the wake of the airfoil and also show the presence of a leading edge flow structure on the airfoil. This is contrary to the quasi-inverse design specification which had a zero-leading edge shedding prescription. It is unclear why there is shedding from the leading edge in the actual flow.

IV.C. Three-Dimensional Wing Studies

We have performed a preliminary computational analysis of flow structure generation on three-dimensional optimal flapping wings at cruising flight speeds using the multi-fidelity framework presented earlier. For these preliminary computations, we chose simple harmonic flapping motions hinged about the wing root. In these cases, we used our quasi-inverse doublet lattice method to determine optimal wing shapes. A series of five different cases were examined:

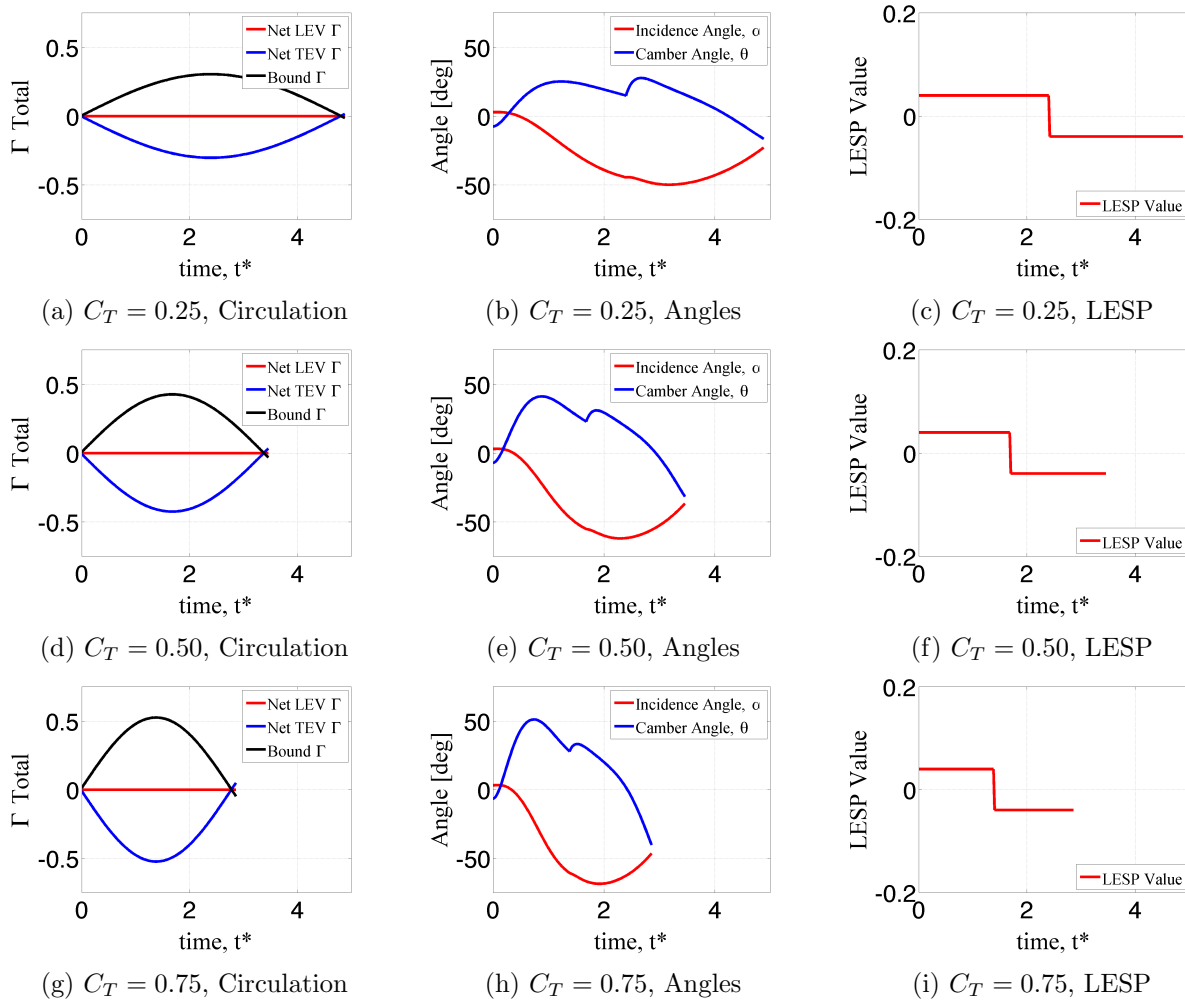


Figure 19. The quasi-inverse design result for $C_T = 0.25, 0.50$ and 0.75 .

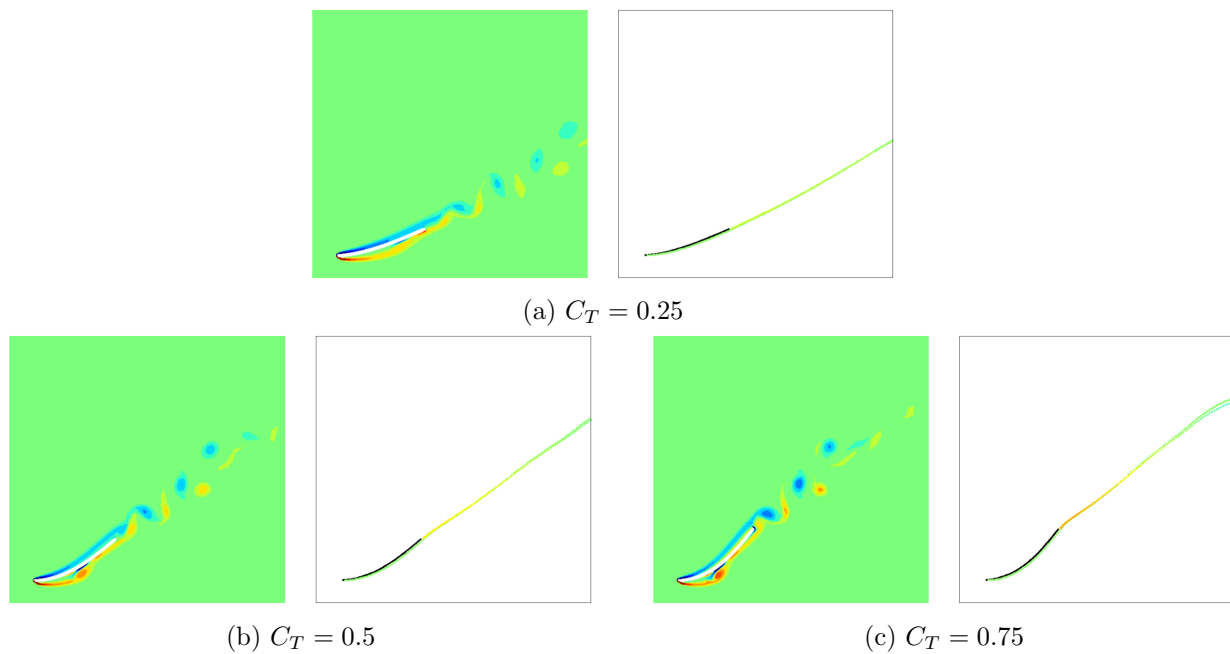


Figure 20. The end of the down-stroke motion, with flowfields predicted using (left) CFD and (right) thin airfoil theory.

1. **Case A:** In this case, the airfoil section at each spanwise wing station had a prescribed zero camber. The spanwise twist angle for the case was determined by ensuring that the shed vorticity matched the wake-only result for that particular timestep in the flapping cycle.
2. **Case B:** In this case, the airfoil section at each spanwise wing station was prescribed to dynamically adjust so that the incident flow was aligned with the leading edge of the wing. This condition is analogous to an LESP value of zero in the two-dimensional setting. The spanwise twist angle was subsequently determined to ensure that the shed vorticity matched the wake-only result for that particular timestep in the flapping cycle.
3. **Case C:** In this case, the airfoil section at each spanwise wing station was prescribed to have a camber of 75% of the maximum spanwise camber recorded in Case B. This camber was fixed at the particular spanwise section for the entire flapping cycle. This cambering strategy was implemented to achieve a simple camber at each spanwise station while still maintaining an LESP value less than or close to the critical value. The spanwise twist angle was determined so that the trailing edge shed vorticity matched the target wake.
4. **Case D:** In this case, the spanwise camber distribution from Case C was adopted and modified such that the camber from that case was reduced linearly from the root of the wing to the tip of the wing. at the root of the wing, the camber was 100% of that in Case C; however, at the tip of the wing the camber was 25% less than that in Case C. This camber distribution was prescribed in order to make the flow leading edge incidence angle more aggressive toward the wingtip. The goal of this geometry prescription was to gradually increase the LESP value along the span of the wing from root to tip, encouraging the generation of increasingly stronger leading edge flow structures toward the wing tips.
5. **Case E:** In this case, the spanwise camber distribution from Case C was adopted and modified such that the camber from that case was reduced quadratically from the root of the wing to the tip of the wing. at the root of the wing, the camber was 100% of that in Case C; however, at the tip of the wing the camber was 25% less than that in Case C. This camber distribution was prescribed in order to make the flow leading edge incidence angle even more aggressive toward the wingtip than in Case D. The goal of this geometry prescription was to aggressively increase the LESP value along the span of the wing from root to tip, once again encouraging the generation of increasingly stronger leading edge flow structures toward the wing tips.

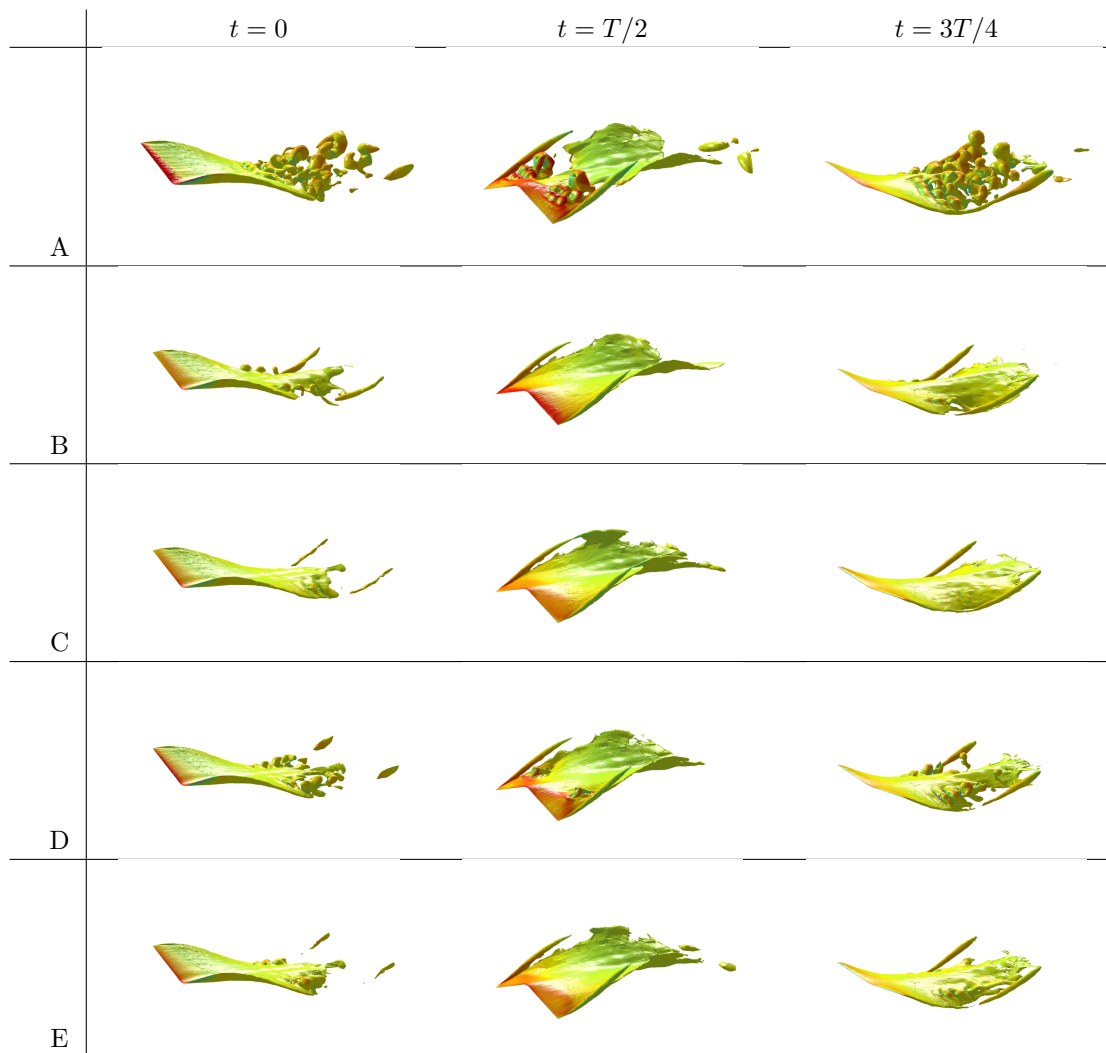


Figure 21. The CFD computed flowfield around several different wings designed using our multi-fidelity framework. Wings A-E are linearly tapered wings. Wing A has a zero-camber strategy. Wing B has a camber that adjusts dynamically such that the leading edge of the wing aligns with the onset flow. Wing C has a prescribed camber that approximately corresponds to the optimal fixed leading edge incidence angle during the downstroke. Wing D is a modified version of wing C, with the incidence angle becoming more aggressive linearly toward the tip, and Wing E is a modified version of wing C, but with the leading edge incidence angle becoming more aggressive quadratically from root to tip. We can see from these examples that different near-wing flow structures are present for each wing. Wing A shows a strong leading edge vortex that sheds during the downstroke. Wings D and E exhibit weaker leading edge vortices near the wing tips that shed after the downstroke is complete. Wings B and C show no leading edge flow structures.

The results of a series of different wing cambering strategies are shown in figure 21. The results from Case A show that a strong leading edge flow structure is generated through the downstroke portion of the flapping cycle. This strong leading edge shedding results in separated flow at the end of the downstroke. In Case B, as might be expected, the alignment of the leading edge with the incident flow produces an attached flow throughout the upstroke and downstroke. Case C is similar to Case B in that the flow remains largely attached through the flapping cycle. This is likely due to (a) the range of LESP values between the maximum and minimum critical LESP values and (b) the downwash from the trailing wake system. Case D and Case E are the cases where leading edge angle has been modulated in order to generate leading edge flow structures. In both of these cases, we have successfully generated a leading edge flow structure in the outboard portion of the wing, where the leading edge angle is more aggressive. In Case D the leading edge flow structure is shed in the final 1/3 of the downstroke; whereas, in case E the leading edge flow structure persists for the entire downstroke. We hypothesize that the leading edge angle in Case D is more aggressive inboard (due to the linear variation of the leading edge angle), and as such, the leading edge flow structure grows more rapidly and sheds earlier. The results of this three-dimensional study indicate that camber can be used to modulate the existence and development of leading edge vortices in three-dimensions.

V. Conclusions and Future Work

The present studies have demonstrated a quasi-inverse, design based approach towards studying and understanding leading edge shedding and leading edge vortex development and evolution in two- and three-dimensions. Our design approach examines the leading and trailing edge vorticity shedding rates as the target of the computation, and determines the airfoil or wing shape that will achieve those shedding rates. This is a unique approach to the problem, as we are effectively designing the wing to accomplish the desired fluid dynamics behavior. This approach allows us to tune the shedding rate and accomplish the desired flow structures around and behind the wing, which may be useful for achieving efficient flight at lower Reynolds numbers. The preliminary results we presented in this paper show significant promise for further understanding LEV development and evolution. For example, we have observed from the cases we have run, that the value and sign of the wing-bound circulation has some impact on whether an LEV is formed or not. In addition, we have been able to show a strong relationship between the airfoil leading edge angle and the shedding strength (and the eventual strength of the LEV).

We plan to extend the use of the leading edge shedding parameter to three dimensions where similar quasi-inverse design approaches could yield a deeper understanding of the variables governing three-dimensional leading edge vortices. In addition, we hope to continue to explore the development of LEVs in the laboratory using computationally derived wing models to further validate the results of this design approach and to deeper understand LEV evolution.

References

- ¹Ellington, C. P., Van Den Berg, C., Willmott, A. P., and Thomas, A. L., "Leading-edge vortices in insect flight," 1996.
- ²Dickinson, M. H. and Gotz, K. G., "Unsteady aerodynamic performance of model wings at low Reynolds numbers," *Journal of Experimental Biology*, Vol. 174, No. 1, 1993, pp. 45–64.
- ³Birch, J. M. and Dickinson, M. H., "Spanwise flow and the attachment of the leading-edge vortex on insect wings," *Nature*, Vol. 412, No. 6848, 2001, pp. 729–733.
- ⁴Birch, J. M. and Dickinson, M. H., "The influence of wing–wake interactions on the production of aerodynamic forces in flapping flight," *Journal of Experimental Biology*, Vol. 206, No. 13, 2003, pp. 2257–2272.
- ⁵Van Den Berg, C. and Ellington, C. P., "The three-dimensional leading-edge vortex of a hovering model hawkmoth," *Philosophical Transactions of the Royal Society of London. Series B: Biological Sciences*, Vol. 352, No. 1351, 1997, pp. 329–340.
- ⁶Dickinson, M. H., Lehmann, F.-O., and Sane, S. P., "Wing rotation and the aerodynamic basis of insect flight," *Science*, Vol. 284, No. 5422, 1999, pp. 1954–1960.
- ⁷Bomphrey, R. J., Taylor, G. K., and Thomas, A. L., "Smoke visualization of free-flying bumblebees indicates independent leading-edge vortices on each wing pair," *Experiments in fluids*, Vol. 46, No. 5, 2009, pp. 811–821.
- ⁸Birch, J. M., Dickson, W. B., and Dickinson, M. H., "Force production and flow structure of the leading edge vortex on flapping wings at high and low Reynolds numbers," *Journal of Experimental Biology*, Vol. 207, No. 7, 2004, pp. 1063–1072.
- ⁹Coloni, T. and Williams, D. R., "Control of vortex shedding on two- and three-dimensional aerofoils," *Philosophical Transactions of the Royal Society A: Mathematical, Physical and Engineering Sciences*, Vol. 369, No. 1940, 2011, pp. 1525–1539.
- ¹⁰Chen, K. K., Coloni, T., and Taira, K., "The leading-edge vortex and quasisteady vortex shedding on an accelerating plate," *Physics of fluids*, Vol. 22, 2010, pp. 033601.
- ¹¹Koehler, C., Wischgoll, T., Dong, H., and Gaston, Z., "Vortex Visualization in Ultra Low Reynolds Number Insect Flight," *Visualization and Computer Graphics, IEEE Transactions on*, Vol. 17, No. 12, 2011, pp. 2071–2079.
- ¹²Shyy, W. and Liu, H., "Flapping Wings and Aerodynamic Lift: The Role of Leading-Edge Vortices," *AIAA Journal*, Vol. 45, 2007, pp. 2817–2819.
- ¹³Dickinson, M., "Animal locomotion: a new spin on bat flight," *Current Biology*, Vol. 18, No. 11, 2008, pp. R468–R470.
- ¹⁴Mujres, F., Johansson, L., Barfield, R., Wolf, M., Spedding, G., and Hedenström, A., "Leading-edge vortex improves lift in slow-flying bats," *Science*, Vol. 319, No. 5867, 2008, pp. 1250–1253.
- ¹⁵Hedenström, A. and Spedding, G., "Beyond robins: aerodynamic analyses of animal flight," *Journal of The Royal Society Interface*, Vol. 5, No. 23, 2008, pp. 595–601.
- ¹⁶Videler, J., Stamhuis, E., and Povel, G., "Leading-edge vortex lifts swifts," *Science*, Vol. 306, No. 5703, 2004, pp. 1960–1962.
- ¹⁷Eldredge, J., Wang, C., and Ol, M., "A Computational Study of a Canonical Pitch-up, Pitch-down Wing Maneuver," AIAA-2009-3687.
- ¹⁸Ol, M. V., Altman, A., Eldredge, J. D., Garmann, D. J., and Lian, Y., "Resume of the AIAA FDTC Low Reynolds Number Discussion Group – Canonical Cases," *48th AIAA Aerospace Sciences Meeting and Exhibit, Orlando, Florida*, January 2010.
- ¹⁹Katz, J. and Plotkin, A., *Low-Speed Aerodynamics*, Cambridge University Press, 2001.
- ²⁰Willis, D. J., Peraire, J., Drela, M., and White, J. K., "A numerical exploration of parameter dependence in power optimal flapping flight," *24th AIAA Applied Aerodynamics Conference, San Francisco, California*, June 2006, AIAA-2006-2994.
- ²¹Peraire, J. and Persson, P.-O., "The compact discontinuous Galerkin (CDG) method for elliptic problems," *SIAM J. Sci. Comput.*, Vol. 30, No. 4, 2008, pp. 1806–1824.
- ²²Willis, D. J., Israeli, E. R., Persson, P.-O., Drela, M., and Peraire, J., "Multifidelity Approaches for the Computational Analysis and Design of Effective Flapping Wing Vehicles," *46th AIAA Aerospace Sciences Meeting and Exhibit, Reno, Nevada*, January 2008, AIAA-2008-518.
- ²³Hall, K., Pigott, S., and Hall, S., "Power requirements for large-amplitude flapping flight," *Journal of Aircraft*, Vol. 35, No. 3, May–June 1998, pp. 352–361, AIAA 35th Aerospace Science Meeting / Nonlinear Dynamical Systems Symposium, RENO, NEVADA, JAN 06-10, 1997.
- ²⁴Salehipour, H. and Willis, D. J., "A coupled kinematics and energetics model for flapping flight," *48th AIAA Aerospace Sciences Meeting and Exhibit, Orlando, Florida*, January 2010, AIAA-2010-1229.
- ²⁵Ramesh, K., Gopalathnam, A., Ol, M., Granlund, K., and Edwards, J., "Augmentation of Inviscid Airfoil Theory to Predict and Model 2D Unsteady Vortex Dominated Flows," *41st AIAA Fluid Dynamics Conference and Exhibit*, June 2011.
- ²⁶Ramesh, K., Gopalathnam, A., Edwards, J., Ol, M., and Granlund, K., "Theoretical, Computational and Experimental Studies of a Flat Plate Undergoing High-Amplitude Pitching Motion," *49th AIAA Aerospace Sciences Meeting*, January 2011.
- ²⁷Ramesh, K., Gopalathnam, A., Granlund, K., Ol, M., and Edwards, J., "Theoretical Modeling of Leading Edge Vortices Using the Leading Edge Suction Parameter," *30th AIAA Applied Aerodynamics Conference*, June 2012.
- ²⁸Drela, M., "XFOIL: An Analysis and Design System for Low Reynolds Number Airfoils," *Lecture Notes in Engineering*, Vol. 54, 1989, pp. 1–12.
- ²⁹Salehipour, H. and Willis, D. J., "A Novel Energetics Model for Examining Flapping Flight," *ECCOMAS CFD 2010 conference in Lisbon, Portugal*, June 2010.
- ³⁰Willis, D. J. and Salehipour, H., "A Multi-fidelity Framework for Designing Compliant Flapping Wings," *ECCOMAS CFD 2010 conference in Lisbon, Portugal*, June 2010.
- ³¹Willis, D. J. and Salehipour, H., "Preliminary Design of Three-Dimensional Flapping Wings from a Wake-Only Energetics Model," *AIAA Atmospheric Flight Mechanics Conference, Toronto, Ontario*, August 2010, AIAA-2010-7630.
- ³²Persson, P.-O. and Willis, D. J., "High Fidelity Simulations of Flapping Wings Designed for Energetically Optimal Flight," *49th AIAA Aerospace Sciences Meeting and Exhibit, Orlando, Florida*, January 2011, AIAA-2011-568.

- ³³Persson, P.-O., Willis, D. J., and Peraire, J., “Numerical simulation of flapping wings using a panel method and a high-order Navier-Stokes solver,” *Internat. J. Numer. Methods Engrg.*, Vol. 89, No. 10, 2012, pp. 1296–1316.
- ³⁴Frink, N. T. and Lamar, J. E., “Water-tunnel and analytical investigation of the effect of strake design variables on strake vortex breakdown characteristics,” *NASA Technical Paper 1676*, 1980.
- ³⁵Oi, M. V., “An experimental investigation of leading edge vortices and passage to stall of nonslender delta wings,” Tech. rep., 2003, RTO-MP-069(I).
- ³⁶Wood, R. M., Byrd, J. E., and Wesselmann, G. F., *Influence of airfoil geometry on delta wing leading-edge vortices and vortex-induced aerodynamics at supersonic speeds*, Vol. 3105, National Aeronautics and Space Administration, Office of Management, Scientific and Technical Information Program, 1992.
- ³⁷Mittal, R. and Iaccarino, G., “Immersed boundary methods,” *Annual review of fluid mechanics. Vol. 37*, Vol. 37 of *Annu. Rev. Fluid Mech.*, Annual Reviews, Palo Alto, CA, 2005, pp. 239–261.
- ³⁸Lu, Y., Shen, G. X., and Lai, G. J., “Dual leading-edge vortices on flapping wings,” *Journal of experimental biology*, Vol. 209, No. 24, 2006, pp. 5005–5016.
- ³⁹Isaac, K. M., Rolwes, J., and Colozza, A., “Unsteady Flow Features of a Flapping and Pitching Wing at Low Reynolds Number,” *AIAA Paper*, Vol. 3145, 2006.
- ⁴⁰Baik, Y. S., Aono, H., Rausch, J. M., Bernal, L. P., Shyy, W., and Oi, M. V., “Experimental Study of a Rapidly Pitched Flat Plate at Low Reynolds Number,” *40th AIAA Fluid Dynamics Conference and Exhibit*, 2010.
- ⁴¹Nakamura, Y., Ohya, Y., and Tsuruta, H., “Experiments on vortex shedding from flat plates with square leading and trailing edges,” *Journal of Fluid Mechanics*, Vol. 222, 1991, pp. 437–447.
- ⁴²Widnall, S. E., “The structure and dynamics of vortex filaments,” *Annual Review of Fluid Mechanics*, Vol. 7, No. 1, 1975, pp. 141–165.
- ⁴³Rockwell, D., “Vortex-body interactions,” *Annual review of fluid mechanics*, Vol. 30, No. 1, 1998, pp. 199–229.
- ⁴⁴Sørensen, J. N., “Instability of helical tip vortices in rotor wakes,” *Journal of Fluid Mechanics*, Vol. 682, 2011, pp. 1.
- ⁴⁵Widnall, S. E., Bliss, D. B., and Tsai, C.-Y., “The instability of short waves on a vortex ring,” *Journal of Fluid Mechanics*, Vol. 66, No. 1, 1974, pp. 35–47.
- ⁴⁶Taylor, G. K., Nudds, R. L., and Thomas, A. L., “Flying and swimming animals cruise at a Strouhal number tuned for high power efficiency,” *Nature*, Vol. 425, No. 6959, 2003, pp. 707–711.
- ⁴⁷Israeli, E., *Simulations of a passively actuated oscillating airfoil using a discontinuous Galerkin method*, Master’s thesis, Massachusetts Institute of Technology, 2008.
- ⁴⁸Iriarte-Díaz, J., Riskin, D. K., Willis, D. J., Breuer, K. S., and Swartz, S. M., “Whole-body kinematics of a fruit bat reveal the influence of wing inertia on body accelerations,” *The Journal of experimental biology*, Vol. 214, No. 9, 2011, pp. 1546–1553.
- ⁴⁹Riskin, D. K., Willis, D. J., Iriarte-Díaz, J., Hedrick, T. L., Kostandov, M., Chen, J., Laidlaw, D. H., Breuer, K. S., and Swartz, S. M., “Quantifying the complexity of bat wing kinematics,” *Journal of Theoretical Biology*, Vol. 254, No. 3, 2008, pp. 604–615.
- ⁵⁰Willis, D., Kostandov, M., Riskin, D., Laidlaw, D., Breuer, K., and Swartz, S., “Modeling the Flight of a Bat,” *Science Magazine*, Vol. 317, 2007, pp. 1858–1863, First Place, NSF-Science Magazine Visualization Challenge.
- ⁵¹Willis, D. J., Peraire, J., and White, J. K., “A combined pFFT-multipole tree code, unsteady panel method with vortex particle wakes,” *Internat. J. Numer. Methods Fluids*, Vol. 53, No. 8, 2007, pp. 1399–1422.
- ⁵²Phillips, J. and White, J., “A Precorrected-FFT Method for Electrostatic Analysis of Complicated 3-D Structures,” *IEEE Transactions On Computer Aided Design of Integrated Circuits and Systems*, Vol. 16, 1997.
- ⁵³Greengard, L., *The rapid evaluation of potential fields in particle systems*, ACM Distinguished Dissertations, MIT Press, Cambridge, MA, 1988.
- ⁵⁴Childress, S., *An introduction to theoretical fluid mechanics*, American Mathematical Society, 2009.
- ⁵⁵Vest, M. and Katz, J., “Aerodynamics of a Flapping-Wing Micro UAV,” *37th Aerospace Sciences Meeting in Reno, NV*, January 1999, AIAA 99-0994.